

# Development of an ecophysiology module in the GEOS-Chem chemical transport model version 12.2.0 to represent biosphere–atmosphere fluxes relevant for ozone air quality

Joey C. Y. Lam<sup>1</sup>, Amos P. K. Tai<sup>1,2</sup>, Jason A. Ducker<sup>3,4</sup>, and Christopher D. Holmes<sup>3</sup>

<sup>1</sup> Earth System Science Programme and Graduate Division of Earth and Atmospheric Sciences, Faculty of Science, The Chinese University of Hong Kong, Sha Tin, Hong Kong

<sup>2</sup> State Key Laboratory of Agrobiotechnology, and Institute of Environment, Energy and Sustainability, The Chinese University of Hong Kong, Sha Tin, Hong Kong

<sup>3</sup> Department of Earth, Ocean and Atmospheric Science, Florida State University, Tallahassee, Florida, USA

<sup>4</sup> Lynker Technologies, LLC, Leesburg, Virginia, USA

Correspondence to: Amos P. K. Tai (amostai@cuhk.edu.hk)

**Abstract.** Ground-level ozone (O<sub>3</sub>) is a major air pollutant that adversely affects human health and ecosystem productivity. Removal of tropospheric O<sub>3</sub> by plant stomatal uptake can in turn cause damage to plant tissues with ramifications for ecosystem and crop health. In many atmospheric and land surface models, the functionality of stomata opening is represented by a bulk stomatal conductance, which is often semi-empirically parameterized, and highly fitted to historical observations. A lack of mechanistic linkage to ecophysiological processes such as photosynthesis may render models inadequate to represent plant-mediated responses of atmospheric chemistry to long-term changes in CO<sub>2</sub>, climate and short-lived air pollutant concentrations. A new ecophysiology module was thus developed to mechanistically simulate land–atmosphere exchange of important gas species in GEOS-Chem, a chemical transport model widely used in atmospheric chemistry studies. The implementation not only allows dry deposition to be coupled with plant ecophysiology, but also enables plant and crop productivity and functions to respond dynamically to atmospheric chemical changes. We conduct simulations to evaluate the effects of the ecophysiology module on simulated dry deposition velocity and concentration of surface O<sub>3</sub> against an observation-derived dataset known as SynFlux. Our estimated stomatal conductance and dry deposition velocity of O<sub>3</sub> are close to SynFlux with root-mean-squared errors (RMSE) below 0.3 cm s<sup>-1</sup> across different plant functional types (PFTs), despite an overall positive bias in surface O<sub>3</sub> concentration (by up to 16 ppbv). Representing ecophysiology was found to reduce the simulated biases in deposition fluxes from the prior model, but worsen the positive biases in simulated O<sub>3</sub> concentrations. The increase in positive concentration biases is mostly attributable to the ecophysiology-based stomatal conductance being generally smaller (and closer to SynFlux values) than that estimated by the prior semi-empirical formulation, calling for further improvements in non-stomatal depositional and non-depositional processes relevant for O<sub>3</sub> simulations. Estimated global O<sub>3</sub> deposition flux is 864 Tg O<sub>3</sub> yr<sup>-1</sup> with GEOS-Chem, and the new module decreases this estimate by 92 Tg O<sub>3</sub> yr<sup>-1</sup>. Estimated global gross primary product (GPP) without O<sub>3</sub> damage is 119 Pg C yr<sup>-1</sup>. O<sub>3</sub>-induced reduction in GPP is 4.2 Pg C yr<sup>-1</sup> (3.5%). An elevated CO<sub>2</sub> scenario (580 ppm) yields higher global GPP (+16.8%) and lower global O<sub>3</sub> depositional sink (–3.3%). Global isoprene emission simulated

Deleted: agricultural

Deleted: air pollutants including

Deleted: from the atmosphere

Deleted: vegetation is controlled mostly by the process of dry deposition, an important component of which is

Deleted: that

Deleted: openness of plant

Deleted:

Deleted: insufficient

Deleted: We adopted the formulations from the Joint UK Land Environmental Simulator (JULES) to couple photosynthesis rate, bulk stomatal conductance and isoprene emission rate dynamically.

Deleted: The research questions of this study include: 1) how the new ecophysiology module compares with the prior, semi-empirical parameterization in terms of simulating concentration and dry deposition velocity of O<sub>3</sub> with respect to site measurement-based estimates; and 2) whether the ecophysiology module simulates vegetation productivity, dry deposition, isoprene emission rate and O<sub>3</sub>–vegetation interactions reasonably under a present-day and an elevated CO<sub>2</sub> concentration.

Deleted: is

Deleted: dry deposition velocity

Deleted: ranging from 0.1 to 0.2

Deleted: , with an

Deleted: damage

Deleted: on

Deleted: of

Deleted:

with a photosynthesis-based scheme is 317.9 Tg C yr<sup>-1</sup>, which is 31.2 Tg C yr<sup>-1</sup> (-8.9%) less than that calculated using the MEGAN emission algorithm. This new model development dynamically represents the two-way interactions between vegetation and air pollutants, and thus provides a unique capability in evaluating vegetation-mediated processes and feedbacks that can shape atmospheric chemistry and air quality, as well as pollutant impacts on vegetation health, especially for any timescales shorter than the multidecadal timescale.

**Deleted:** pollutant impacts on vegetation health and

**Deleted:** processes

## 1 Introduction

Surface ozone (O<sub>3</sub>) is a strong oxidative species and is harmful to human respiratory system (e.g., Anenberg et al., 2010) and vegetation, with ramifications to boundary-layer meteorology (e.g. Sadiq et al., 2017), water and carbon cycle (e.g. Sitch et al. 2007; Lombardozi et al., 2015), crop production (e.g. Avnery et al, 2011; Ainsworth et al, 2012; Mills et al, 2018) and food security (e.g. Tai et al, 2014; Tai and Val Martin, 2017). Tropospheric O<sub>3</sub> is not emitted directly into the atmosphere, but is generated by photochemical oxidation of precursor gases including carbon monoxide (CO), methane (CH<sub>4</sub>), and other volatile organic compounds (VOCs) under the presence of nitrogen oxides (NO<sub>x</sub>= NO + NO<sub>2</sub>); while many of these precursors are mostly from anthropogenic sources, biogenic VOCs (BVOCs) are globally important components of VOCs. The most abundant species of BVOCs is isoprene emitted mostly from land vegetation. Meanwhile, O<sub>3</sub> is mainly removed by chemical loss as well as via dry deposition, whereby vegetation also plays an important role. Therefore, surface O<sub>3</sub> can be significantly modulated by vegetation through isoprene emission and dry deposition. Further, strong positive correlations between surface ozone and temperature have been well documented and attributed to multiple factors including higher isoprene emission and faster decomposition of PAN back to NO<sub>x</sub> at higher temperatures (e.g., Jacob and Winner, 2009). Vegetation can therefore further modulate surface O<sub>3</sub> by regulating surface energy balance and surface temperature via transpiration and changing the land surface albedo (e.g., Wang et al., 2020).

**Deleted:** Avnery et al, 2011

Isoprene emission is one of the pathways via which vegetation affects surface O<sub>3</sub> concentration. Isoprene comprises about half of the global BVOC emissions and is mainly produced by terrestrial vegetation. It can be photochemically oxidized under the presence of NO<sub>x</sub> to form surface O<sub>3</sub>. Therefore, in a VOC-limited environment, more surface O<sub>3</sub> is produced following an increase in isoprene emission rate. However, in a NO<sub>x</sub>-limited environment, isoprene can reduce O<sub>3</sub> concentration either by directly reacting with O<sub>3</sub> or sequestering NO<sub>x</sub> as isoprene nitrate (e.g., Sanderson et al., 2003; Tai et al., 2013). An increase in isoprene emission rate could thus reduce surface O<sub>3</sub> concentration. Isoprene emission rate is dependent on both the vegetation type and a complex array of environmental variables, such as sunlight, temperature, soil moisture, and ambient CO<sub>2</sub> concentration. Many previous studies have used various models to estimate the global biogenic isoprene emission budget (e.g., Arneth et al., 2007; Pacifico et al., 2011; Guenther et al., 2012; Unger, 2013), which is about 300–500 Tg C yr<sup>-1</sup>.

**Deleted:** whereby gases and particles in the atmosphere adhere to or are absorbed by any surface

**Deleted:**

**Deleted:** e

**Deleted:** soil water

**Deleted:** or

**Deleted:** via gravitational settling or turbulent transfer

Dry deposition is a process of uptake at the Earth's surface by water bodies, soil and vegetation. It is often modeled by a resistor-in-series model, analogous to the concept of electric circuit (Wesely, 1989). Under this framework, gaseous species in the atmosphere will go through different layers of air before depositing on a surface, and the flux across each layer

is controlled by a resistance. There are three major resistances in this scheme: aerodynamic resistance ( $r_a$ ), quasilaminar sub-layer resistance ( $r_b$ ) and surface resistance ( $r_c$ ). For a vegetated surface,  $r_c$  is further divided into different components to represent the uptake via different parts of plant canopy and soil surface. The bulk canopy stomatal resistance  $r_s$ , which describes the bulk property of plant stomata, is frequently the component that contributes the most to the variability of  $r_c$ . Plants modulate their stomata to maximize CO<sub>2</sub> capture and minimize water loss, so stomatal behavior is tightly connected to photosynthesis and depends on environmental conditions such as photosynthetically active radiation (PAR), humidity, temperature, and soil moisture. The openness of stomata is represented by the stomatal conductance,  $g_s$ , which is the reciprocal of  $r_s$ . The bulk canopy stomatal conductance aggregates the behavior of all stomata inside a canopy. Therefore, smaller resistance or larger conductance represents more open stomata inside a canopy and allows a larger material flux, and vice versa. In many chemical transport models (CTMs), the response of  $r_s$  to environmental variables is not fully captured. For example, the parameterization of  $r_s$  in Wesely (1989) as commonly implemented in various CTMs includes the dependence on PAR and temperature only. However, atmospheric moisture content is also an essential factor contributing to the variability of  $r_s$ . Franks and Farquhar (1999) showed that a doubling of vapor pressure deficit (VPD) reduces  $r_s$  by more than 20%. Kavassalis and Murphy (2017) showed that VPD is a strong predictor of midday O<sub>3</sub> in the US, suggesting that [VPD-dependent dry deposition plays an important role in producing day-to-day O<sub>3</sub> variability](#). Various mechanistic approaches that include VPD in the formulation of  $r_s$  have been suggested (e.g., Leuning, 1995; Medlyn et al., 2011; De Kauwe et al., 2015). These formulations are ultimately connected to the modeling of plant ecophysiology.

Ecophysiology refers to the study of interactions between physiological processes of plants and the environment. Photosynthesis fixes atmospheric CO<sub>2</sub> into terrestrial ecosystems and thereby facilitates the exchange of water, CO<sub>2</sub> and energy between plants and the environment. Formulations to model photosynthesis have been developed by Collatz et al. (1991) and Collatz et al. (1992) for C<sub>3</sub> and C<sub>4</sub> plants, respectively, and widely used in different numerical models (e.g. Sellers et al., 1996; Clark et al. 2011). When plant stomata open to absorb CO<sub>2</sub>, water vapor diffuses from the leaf interior to the atmosphere in the process known as transpiration, with ramifications for canopy micrometeorology and boundary-layer meteorology. Stomatal behavior is regulated by a compromise between photosynthetic pathways and transpiration. Larger stomatal conductance results in larger photosynthetic uptake of CO<sub>2</sub> but also larger water loss through transpiration, and plants have evolved to strike a balance between the two. The coupling between photosynthesis and stomatal conductance also has implications for their interactions with the environment under dry conditions. For instance, during a drought event, stomatal conductance decreases as plants attempt to reduce water loss. This, in turn, amplifies the drought condition and reduces ecosystem productivity (e.g., Emberson et al., 2013). Plant stomatal behavior also affects biosphere–atmosphere exchange of other gaseous species relevant for atmospheric chemistry. Besides the exchange of water and CO<sub>2</sub>, dry-depositing gaseous species including O<sub>3</sub>, sulfur dioxide (SO<sub>2</sub>) and hydrogen peroxide (H<sub>2</sub>O<sub>2</sub>) can be removed from the atmosphere through plant stomata. Thus, the openness of plant stomata affects the dry deposition flux of these gaseous species, altering concentrations of near-surface air pollutants. For

**Deleted:** vegetation alters O<sub>3</sub> concentration through stomatal regulation...

example, O<sub>3</sub> dry deposition is suppressed during drought events, possibly resulting in higher surface O<sub>3</sub> concentrations (Emmerson et al., 2013; Huang et al., 2016).

O<sub>3</sub>-vegetation interaction is another important topic in plant ecophysiology that is also relevant for atmospheric chemistry. Vegetation not only affects O<sub>3</sub> but is also influenced by O<sub>3</sub>, which can attack and damage plant tissues upon stomatal uptake. When the O<sub>3</sub> flux into plant stomata is small, plants naturally detoxify the oxidative stress from O<sub>3</sub>, but large O<sub>3</sub> flux overwhelms the detoxification capacity and may cause visible foliage injury. Stomata can close, or in some cases become “sluggish” in responding to environmental changes (e.g., Huntingford et al., 2018), as a result of O<sub>3</sub> damage, with ramifications to boundary-layer meteorology, water and carbon cycle, crop production and food security. In particular, it reduces gross primary production (GPP), which is the gross carbon uptake via photosynthesis and a measure of ecosystem productivity. O<sub>3</sub>-induced reduction in GPP is usually less than 10% globally under present-day O<sub>3</sub> concentration, but it can be more than 30% regionally (Lombardozzi et al., 2015; Yue and Unger, 2015). Stomatal control of O<sub>3</sub> uptake also appears to explain the divergent trends in O<sub>3</sub> concentration and plant damage in the recent decade (Ronan et al., 2020). Overall, there are three major feedback pathways that couple surface O<sub>3</sub> to vegetation, whereby O<sub>3</sub> damage on vegetation ultimately affects O<sub>3</sub> itself (Sadiq et al., 2017; Zhou et al., 2018; Wang et al., 2020). First, long-term decline in GPP and leaf area index (LAI) due to O<sub>3</sub> damage can suppress BVOC emissions, thereby modulating surface O<sub>3</sub>; in a high-NO<sub>x</sub> environment, this may reduce O<sub>3</sub> levels, constituting a negative feedback. Second, O<sub>3</sub> damage generally reduces stomatal conductance and thus the dry-depositional flux of O<sub>3</sub>, thereby enhancing surface O<sub>3</sub> concentration (i.e., positive feedback). Finally, O<sub>3</sub> damage can suppress transpiration and the associated evaporative cooling effect, thereby enhancing surface temperature and surface O<sub>3</sub> (i.e., positive feedback).

Rising CO<sub>2</sub> can further complicate O<sub>3</sub>-vegetation interactions. An elevated CO<sub>2</sub> concentration alters plant behaviors and thus atmospheric chemistry via three main pathways. First, plants tend to close their stomata more as the CO<sub>2</sub> diffusive flux increases, and such stomatal responses to changing CO<sub>2</sub> can be described either mechanistically (e.g., Clark et al., 2011) or empirically (e.g., Franks et al., 2013). Dry deposition flux is thus reduced, and the corresponding chemical gas species remain in the atmosphere longer. For example, Sanderson et al. (2007) suggested that O<sub>3</sub> concentration could increase by 8 ppbv under a doubling of present-day CO<sub>2</sub> concentration due to reduced stomatal conductance and dry deposition. A reduction in dry deposition flux of O<sub>3</sub> should imply less O<sub>3</sub> damage on plants, but more O<sub>3</sub> left in the atmosphere in the longer term might offset such benefit. Second, it was shown that isoprene emission can be suppressed by elevated CO<sub>2</sub> (Possell and Hewitt, 2011). In high-NO<sub>x</sub> environments, lower isoprene emission reduces O<sub>3</sub> production rate, but in NO<sub>x</sub>-limited regions such as tropical forests and other remote areas, O<sub>3</sub> concentration may increase (Tai et al., 2013). Finally, higher CO<sub>2</sub> enhances photosynthesis and thus LAI in the long term, and this is known as CO<sub>2</sub> fertilization. This can enhance both dry deposition and isoprene emission, either enhancing or offsetting the previous two effects depending on the O<sub>3</sub> formation regime.

In view of the above, a proper representation of ecophysiological processes has the potential to improve atmospheric chemistry modeling, especially in relation to biosphere-atmosphere exchange. This can be done in various ways. A CTM can be coupled with a land surface or biosphere model within an Earth system framework, whereby atmospheric processes (e.g.,

Deleted:

deposition, emissions) can be linked dynamically to biospheric processes (e.g., photosynthesis, stomatal regulation, soil biogeochemistry). For instance, Sadiq et al. (2017) and Lei et al. (2020) both examined O<sub>3</sub>-vegetation interactions by developing a modeling framework where ozone air quality, ecophysiology and ecosystem structure (e.g., LAI, canopy height) can co-evolve interactively. This approach is particularly useful for examining how ecosystem structure may respond to long-term atmospheric chemical changes over multidecadal timescales. However, the computation of ecosystem structure involves complex representation of plant phenology and biogeochemistry (e.g., allocation, biomass growth, senescence, mortality), which may be unnecessary for problems involving shorter timescales, e.g., seasonal responses of plant-atmosphere interactions and O<sub>3</sub> pollution to droughts or heatwaves (e.g., Emberson et al., 2013). It also introduces extra uncertainties while not necessarily improving model performance in atmospheric chemistry. A more efficient approach is to implement process-based representation of ecophysiology into a CTM. This has been done to various extents in the past; e.g., Zhang et al. (2003) implemented a semi-empirical, multiplicative scheme based on Jarvis (1976) to account for plant responses to varying radiation, temperature, VPD, and soil water stress. However, thus far the variability of  $r_s$  is still often not fully captured in CTMs. A mechanistic approach in modeling  $r_s$  should account for the ecophysiology behind, especially photosynthesis, and therefore better simulate  $r_s$ .

In this study, we developed a new ecophysiology module in the GEOS-Chem chemical transport model to dynamically simulate bulk canopy stomatal conductance  $g_s$  and plant photosynthesis  $A_n$ . Figure 1 summarizes the interactions in the prior GEOS-Chem and in the new ecophysiology module. We highlight that O<sub>3</sub> damage on vegetation is a key component in the model because it allows atmospheric chemistry, in addition to meteorology, to affect plant ecophysiology, and represents a more complete set of two-way interactions and feedback pathways. This development not only provides an alternative to the prior parameterization in the dry deposition module based on Wesely (1989), but also allows biogeoscientists to study the effects of pollutant deposition on plant health, especially when simultaneously influenced by other stresses such as droughts and heatwaves. By considering leaf biochemistry, boundary-layer meteorology, soil moisture stress and O<sub>3</sub> deposition damage, this new module can couple physiological processes to atmospheric chemistry. We particularly aim to address two questions:

1. How does the ecophysiology module compare to the semi-empirical Wesely (1989) parameterization in terms of simulating concentration and dry deposition velocity of O<sub>3</sub>, when compared to estimates based on site measurements?
2. Does the ecophysiology module simulate vegetation productivity, dry deposition, isoprene emission rate and O<sub>3</sub>-vegetation interactions reasonably under a present-day and an elevated CO<sub>2</sub> concentration?

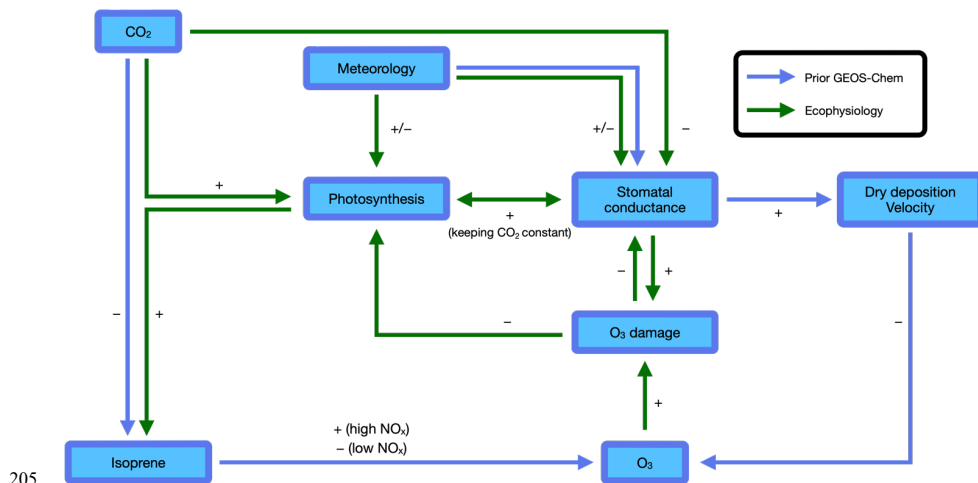
**Deleted:** , but

**Deleted:** ily

**Deleted:** computationally expensive

**Deleted:** that arise from the computation of ecosystem structure, which involves complex representation of plant phenology and biogeochemistry (e.g., allocation, biomass growth, senescence, mortality),

**Deleted:** , and with it



205 **Figure 1: Atmosphere–biosphere interactions represented in the GEOS-Chem chemical transport model. Blue arrows indicate interactions included in the prior GEOS-Chem without ecophysiology. Green arrows indicate interactions added in the new ecophysiology module. The sign associated with each arrow indicates the sign of effect of one factor on another. The two arrows pointing from “Meteorology” to “Stomatal conductance” indicate that the ecophysiology module changes how meteorology affects stomatal**  
 210 **conductance. Other species are also simulated by the GEOS-Chem and may interact with O<sub>3</sub>, but are omitted here for simplicity.**

## 2 Model

### 2.1 Model description

The GEOS-Chem global chemical transport model ([www.geos-chem.org](http://www.geos-chem.org)) version 12.2.0 includes detailed HO<sub>x</sub>–NO<sub>x</sub>–VOC–O<sub>3</sub>–halogen–aerosol tropospheric chemistry (Bey et al., 2001). We conducted simulations at a horizontal resolution of  
 215 2° latitude by 2.5° longitude, driven by assimilated meteorology at an hourly time resolution from the Modern-Era Retrospective analysis for Research and Applications, Version 2 (MERRA-2) (Gelaro et al., 2017) dataset, which is an atmospheric reanalysis dataset that includes assimilation of aerosol observations. Leaf area indices (LAI) are prescribed by a gridded dataset from Yuan et al. (2011), who used gap-filling and smoothing techniques to process MODIS (Moderate Resolution Imaging Spectroradiometer) LAI. Emission data are handled by the Harmonized Emission Component (HEMCO) v2.1 (Keller et al.,  
 220 2014). HEMCO uses anthropogenic emissions of CO, NO<sub>x</sub> and non-methane VOCs (NMVOCs) from the Community Emissions Data System (CEDS) inventory (Hoesly et al., 2018) and the biogenic emissions of NMVOCs are computed by the Model of Emissions of Gases and Aerosols from Nature (MEGAN) version 2.1 (Guenther et al., 2012). Besides the MEGAN emission inventory, we also implemented a photosynthesis-based isoprene emission scheme following Pacifico et al. (2011) as an

alternative. The scheme introduces another pathway of coupling atmospheric chemistry to ecophysiology. The detailed formulation is included in Sect. 2.1.7.

Dry deposition is modeled using the Wesely (1989) scheme, but with  $r_s$  calculated from the new ecophysiology module. It is simulated for every land surface type in the Olson Land Map, which is derived from the USGS global land characteristics database (<https://doi.org/10.5066/F7GB230D>). These land surface types are also mapped into five plant functional types (PFTs), which are used in the ecophysiology module to represent different types of vegetation. The five PFTs are broadleaf tree, needleleaf tree, C<sub>3</sub> grass, C<sub>4</sub> grass, and shrub. Each PFT has a different set of parameters, thus yielding different  $r_s$ . PFT-specific parameters (tabulated in Table S1) are from Clark et al. (2011), Raoult et al. (2016) and Sitch et al. (2007). The module would skip the calculation for a PFT if it does not exist within the grid cell. The ecophysiology module also requires extra soil parameters to calculate soil moisture stress (see Sect. 2.1.5). We used gridded soil parameter data from the Hadley Centre Global Environment Model version 2 – Earth System Model (HadGEM2-ES) to calculate the soil moisture stress function (details in Sect. 2.1.5). Besides  $r_s$ , vegetation-related outputs such as gross photosynthetic uptake of carbon, canopy dark respiration and canopy O<sub>3</sub> uptake are also available. The formulations in the ecophysiology module were adopted from the Joint UK Land Environmental Simulator (JULES) (Best et al., 2011; Clark et al., 2011). [Important ones are included below and others are detailed in the supplementary materials.](#)

### 2.1.1 Leaf biochemistry

Formulations of photosynthesis rates for C<sub>3</sub> and C<sub>4</sub> plants were derived from leaf biochemistry and formulated as in Collatz et al. (1991) and Collatz et al. (1992), respectively. It is calculated from the three potentially limiting rates, [each as a function of  \$c\_i\$  and some other meteorological variables \(see supplementary materials\).](#)

The leaf-level net photosynthesis ( $A_n$ ,  $\mu\text{mol CO}_2 \text{ m}^{-2} \text{ s}^{-1}$ ) is calculated as a smoothed minimum (see supplementary materials) of the three potentially limiting rates ( $W_c$ ,  $W_i$ ,  $W_e$ ,  $\mu\text{mol CO}_2 \text{ m}^{-2} \text{ s}^{-1}$ ) minus dark respiration ( $R_d$ ,  $\mu\text{mol CO}_2 \text{ m}^{-2} \text{ s}^{-1}$ ):

$$A_n = \min(W_c, W_i, W_e) - R_d \quad (1)$$

where  $R_d$  is linearly proportional to  $V_{\text{cmax}}$  by the dark respiration coefficient  $f_d$ :

$$R_d = f_d V_{\text{cmax}} \quad (2)$$

### 2.1.2 Photosynthesis as a diffusive flux

The leaf-level net photosynthesis  $A_n$  can also be represented as a diffusive flux of CO<sub>2</sub> modulated by the leaf-level stomatal conductance  $g_{s0}$  ( $\text{m s}^{-1}$ ). Therefore, we can find  $g_{s0}$  using:

$$g_{s0} = \frac{1.6 \times 10^{-6} A_n}{c_c - c_i} R_* T \quad (3)$$

where  $c_c$  is the canopy CO<sub>2</sub> partial pressure (Pa), 1.6 accounts for different diffusivities of CO<sub>2</sub> and H<sub>2</sub>O through leave stomata,  $R_* = 8.31 \text{ J K}^{-1} \text{ mol}^{-1}$  is the universal molar gas constant, and  $T$  is the canopy air temperature (K). We assume  $c_c$  and  $T$  to be equal to the ambient CO<sub>2</sub> concentration and the 2 m temperature respectively.

Deleted: 8

Deleted: and

Deleted: below

Deleted: Photosynthesis consists of two main stages: the light reaction, where energy from sunlight is harnessed to form high-energy and electron-carrying intermediate molecules known as adenosine triphosphate (ATP) and reduced nicotinamide adenine dinucleotide phosphate (NADPH), and the dark reaction, where ATP and NADPH produced in the light reaction are used to power the reduction of CO<sub>2</sub> to carbohydrates via a biochemical reaction cycle known as the Calvin cycle. The Calvin cycle can further be separated into three phases. The first phase is carboxylation, where CO<sub>2</sub> molecules enter and combine with ribulose-1,5-bisphosphate (RuBP) into a 3-carbon compound. The rate of carboxylation is controlled by an enzyme known as ribulose biphosphate carboxylase/oxygenase (Rubisco), and thus this rate is also known as Rubisco-limited rate. The second phase is reduction, where the three-carbon product is reduced by NADPH and ATP to produce glyceraldehyde 3-phosphate (G3P), some of which then exit the Calvin cycle and are used to synthesize other carbohydrates. The remaining G3P molecules are utilized to regenerate RuBP under the presence of ATP in the final phase known as regeneration. The rates of reduction and regeneration are limited by the availability of ATP and NADPH molecules, and ultimately depend on the utilization rate of G3P, also known as the product-limited rate, and the rate of photon-assimilating reactions in the light reaction, also known as light-limited rate. Plants that follow the above mechanism are called C<sub>3</sub> plants, because CO<sub>2</sub> molecules are synthesized into 3-carbon products directly. There are also C<sub>4</sub> plants, which first incorporate CO<sub>2</sub> into a 4-carbon compound, which is then transported to another cell where CO<sub>2</sub> is released and consumed in the dark reaction.

Deleted: :

Deleted: <#>Rubisco-limited rate:¶

CO<sub>2</sub> assimilation is limited by the availability of CO<sub>2</sub> in intercellular space, the kinetic properties of active sites of Rubisco, and/or the available amount of Rubisco. It is modeled as:¶

(1)¶

where  $V_{\text{cmax}}$  is the maximum carboxylation rate ( $\mu\text{mol CO}_2 \text{ m}^{-2} \text{ s}^{-1}$ ),  $c_i$  and  $o_i$  are the partial pressures (Pa) of CO<sub>2</sub> and O<sub>2</sub> in intercellular space, respectively,  $\Gamma$  is the CO<sub>2</sub> photorespiration compensation point (Pa), and  $K_c$  and  $K_o$  are the Michaelis–Menten coefficients (Pa) for carboxylation and oxygenation, respectively.  $c_i$  is calculated in Sect. 2.1.4.  $o_i$  is assumed to be equal to the partial pressure of O<sub>2</sub> in the lowest model level. Detailed formulations of temperature-dependent parameters are included in the supplementary materials.¶

RuBP-limited rate (light-limited rate): ¶

It describes the regeneration rate of RuBP, which depends on the amount of ATP and NADPH. This ultimately depends on the availability of absorbed photons, and is modeled as:¶

(2)¶

where  $\alpha$  is the quantum efficiency of photosynthesis ( $\text{mol CO}_2 \text{ mol}^{-1} \text{ PAR}$ ),  $c_a = 4.6 \mu\text{mol PAR J}^{-1}$  is a conversion constant, and  $\phi$  is the absorbed photosynthetically active radiation (PAR,  $\text{W m}^{-2}$ ). [1]

Deleted: 4

Deleted: 5

Deleted: 6

### 340 2.1.3 Canopy scaling

A simple big-leaf approach is applied to scale up leaf-level variables to the canopy-level variables. It is assumed that incident light is attenuated by the canopy according to Beer's law:

$$I(L) = I_0 e^{-kL} \quad (4)$$

where  $I(L)$  and  $I_0$  are the irradiance at the height of the canopy with cumulative leaf area index  $L$  and at the top of the canopy, respectively, and  $k$  is the PAR extinction coefficient of the canopy. [Detailed formulations can be found in the supplementary materials.](#)

#### 2.1.4 Stomatal closure parameterization

A third equation by Jacobs (1994) relating  $c_i$  and  $g_s$  via canopy humidity deficit  $D$  ( $\text{kg}_w \text{kg}_a^{-1}$ ) is included to obtain a closed set of equations for  $A_n$ ,  $g_{s0}$  and  $c_w$ . This formulation was discussed in detail by Cox et al. (1998).

$$350 \frac{c_i - \Gamma}{c_c - \Gamma} = f_0 \left( 1 - \frac{D}{D^*} \right) \quad (5)$$

where  $f_0$  and  $D^*$  are PFT-specific parameters.  $D$  is evaluated as the difference between the saturation specific humidity ( $\text{kg}_w \text{kg}_a^{-1}$ ) evaluated at leaf temperature  $T_l$  and the 2 m specific humidity. We assume a thin leaf boundary layer,  $T_l$  would be equal to the 2 m air temperature.

#### 2.1.5 Soil moisture stress

355 Under dry soil conditions,  $A_n$ ,  $R_d$  and  $g_{s0}$  are reduced due to limited availability of water. An extra factor  $\beta_t$ , which ranges from 0 to 1, is multiplied to all three quantities. It is modeled as:

$$\beta_t = \begin{cases} 1 & \text{for } \theta > \theta_c \\ \frac{\theta - \theta_w}{\theta_c - \theta_w} & \text{for } \theta_w < \theta \leq \theta_c \\ 0 & \text{for } \theta \leq \theta_w \end{cases} \quad (6)$$

360 where  $\theta = S \times \theta_s$  is the root zone soil moisture,  $S$  is the root zone soil wetness (in terms of fraction of soil pore space), and  $\theta_s$ ,  $\theta_c$  and  $\theta_w$  are the saturation, critical and wilting soil moisture, respectively. We use the soil ancillary maps that contain  $\theta_s$ ,  $\theta_c$  and  $\theta_w$  at  $0.5^\circ \times 0.5^\circ$  resolution from HadGEM2-ES.

#### 2.1.6 O<sub>3</sub> damage

The O<sub>3</sub> damage scheme in JULES is based on Sitch et al. (2007). When the ambient O<sub>3</sub> concentration is high enough,  $A_n$ ,  $R_d$  and  $g_{s0}$  is further reduced due to O<sub>3</sub> damage on plant cells. An O<sub>3</sub> damage factor  $\beta_{O_3}$ , which ranges from 0 to 1, is multiplied to the three quantities. The damage factor is given by:

$$365 \beta_{O_3} = 1 - a \times \max[F_{O_3} - F_{O_3 \text{ crit}}, 0] \quad (7)$$

Deleted: 7

Deleted: It is also assumed that the in-canopy leaf photosynthetic capacity  $V_{\text{max}}$  at different heights vary proportionally to the in-canopy light profile. Therefore, from Eq. (4), (5) and (6), leaf-level net photosynthesis rate  $A_n$ , dark respiration rate  $R_d$ , and stomatal conductance  $g_{s0}$  also follow the same profile. Integrating over the entire canopy, the canopy-level net photosynthesis  $A_c$ , respiration  $R_{dc}$  and stomatal conductance  $g_s$  are given by:<sup>¶</sup>

(8)<sup>¶</sup>

(9)<sup>¶</sup>

(10)<sup>¶</sup>

where  $L_c$  is the canopy total leaf area index ( $\text{m}^2 \text{m}^{-2}$ ).<sup>¶</sup>

Deleted:  $c$

Deleted: 11

Deleted: 12

Deleted: 13



where  $F_{O_3}$  is the  $O_3$  deposition flux through stomata ( $\text{nmol m}^{-2} \text{s}^{-1}$ ),  $F_{O_3 \text{ crit}}$  is the threshold for stomatal  $O_3$  uptake ( $\text{nmol m}^{-2} \text{s}^{-1}$ ), and  $a$  is the gradient of the  $O_3$  dose response function ( $\text{nmol}^{-1} \text{m}^2 \text{s}$ );  $a$  and  $F_{O_3 \text{ crit}}$  are PFT-specific parameters. There are two sets of values of  $a$  corresponding to “high” and “low” sensitivities. The stomatal  $O_3$  deposition flux is modeled using a flux gradient approach:

$$F_{O_3} = \frac{[O_3]}{r_a + r_b + \kappa_{O_3} r_s} \quad (8)$$

where  $[O_3]$  is the molar concentration of  $O_3$  at the lowest model level,  $r_a$  is the aerodynamic resistance ( $\text{s m}^{-1}$ ),  $r_b$  is the quasi-laminar sublayer resistance,  $r_s = 1 / g_s$  is the stomatal resistance, and  $\kappa_{O_3} = 1.61$  accounts for the relative difference in diffusivities of  $O_3$  and  $H_2O$  through leave stomata. Since  $r_s$  in equation (8) depends on  $\beta_{O_3}$ , equations (7) and (8) can be combined into a quadratic equation and solved analytically to give  $\beta_{O_3}$ .

### 2.1.7. Photosynthesis-dependent isoprene emission

In the default GEOS-Chem, canopy isoprene emission is computed by MEGAN v2.1, which calculates biogenic VOC emissions of various species as functions of canopy-scale PFT-specific emission factors modulated by environmental activity factors to account for changing temperature, light, leaf age and LAI, weighted by the PFT fraction in each grid cell to give the grid cell-level emission fluxes. The activity factors are essentially semi-empirical functions constrained by experimental data, not explicitly linked to mechanistic ecophysiological processes. Here in the ecophysiology module, canopy isoprene emission ( $E_{\text{isoprene}}$ ,  $\text{kg C m}^{-2} \text{s}^{-1}$ ) is linked explicitly to photosynthesis, based on Pacifico et al. (2011):

$$E_{\text{isoprene}} = \text{IEF} \rho_{\text{leaf}} \frac{A_c + R_{dc}}{(A_n)_{\text{st}} + (R_d)_{\text{st}}} f_T f_{\text{CO}_2} \quad (9)$$

where IEF is the PFT-specific isoprene emission factor ( $\mu\text{g C g dw}^{-1} \text{h}^{-1}$ , “dw” means dry weight), i.e., base emission rate of isoprene at the leaf level under standard conditions (i.e., temperature of  $30^\circ\text{C}$ , photosynthetically active radiation of  $1000 \mu\text{mol CO}_2 \text{ m}^{-2} \text{ s}^{-1}$ ,  $\text{CO}_2$  concentration of 370 ppm and without any  $O_3$  damage or soil moisture stress),  $\rho_{\text{leaf}}$  is the dry leaf area density ( $\text{g dw}^{-1} \text{m}^{-2}$ ),  $f_T$  and  $f_{\text{CO}_2}$  are temperature- and  $\text{CO}_2$ -dependent empirical factors to account for variation with changing temperature and  $\text{CO}_2$  level (see supplementary materials for detailed formulations). Variables with subscript “st” are calculated under standard conditions. We note that, as opposed to Pacifico et al. (2011), our model does not capture a reduction in  $c_i$  following soil moisture limitation because we use prescribed 2 m specific humidity data in the meteorological input to calculate  $c_i$ . The effect of soil moisture stress on isoprene emission is only captured in the calculation of  $A_c$  and  $R_{dc}$ . This may lead to a lower isoprene emission rate compared to the original scheme, but direct comparison is not possible due to different input meteorology used in our study.

## 2.2 Experimental design

To evaluate the modeled concentration and dry deposition velocity of  $O_3$ , we conduct four one-year simulations from 1 January 2012 to 1 January 2013 using GEOS-Chem v12.2.0 driven by offline MERRA-2 meteorology. A half-year spin-up

Deleted: 14

Deleted: 14

Deleted: 13

Deleted: 14

Deleted: ¶

#### 2.1.7 Open vs. closed stomata¶

It is important to note that open and closed stomata are treated differently in the module. Open stomata follow the processes described above. Closed stomata are assigned a minimum value of stomatal conductance  $g_{\text{min}} = 10^{-6} \text{ m s}^{-1}$ . Photosynthesis and  $O_3$  deposition cannot occur, and thus  $A_n$  is only affected by  $R_d$  and  $\beta_i$ :  
(15)¶

Closed stomata are determined by¶  
, which indicates that  $g_{\text{st}}$  is close to zero and the associated fluxes can be neglected,¶

, which indicates that photosynthesis is not effective, and thus plants close the stomata.¶

, which implies from Eq. (11), hence there is no net uptake of  $\text{CO}_2$  across stomata,¶

, which implies a dry soil condition inhibiting photosynthesis, or¶  
, which implies that PAR is not available for photosynthesis.¶

Deleted: 8

Deleted: prior

Deleted: 16

Deleted: S

Deleted: .

Deleted:  $f_T$  and  $f_{\text{CO}_2}$  are calculated as:¶

(17)¶

(18)¶

where  $a_T = 0.1 \text{ K}^{-1}$ ,  $T_{st} = 300 \text{ K}$ ,  $c_i$  is the partial pressure of  $\text{CO}_2$  in the intercellular space.

is conducted before the simulation period. Table 1 summarizes the configurations of each simulation. A control case (case 0) uses the GEOS-Chem v12.2.0 with prior input configuration while other three (cases 1a–c) use the modified GEOS-Chem with ecophysiology module turned on. Each of the three cases use different O<sub>3</sub> damage sensitivities. We then compare the modeled concentration and dry deposition velocity of O<sub>3</sub> against site observations. Year 2012 is chosen as the simulation year to maximize the number of observations our results can be evaluated against.

**Table 1: Configuration of the first set of simulations that evaluate the modeled concentration and dry deposition velocity of ozone (O<sub>3</sub>).**

Case	[CO <sub>2</sub> ] (ppmv)	Ecophysiology module	O <sub>3</sub> damage scheme and sensitivity
0	390	Off	No O <sub>3</sub> damage applied
1a	390	On	No O <sub>3</sub> damage applied
1b	390	On	Sitch et al. (2007), low sensitivity
1c	390	On	Sitch et al. (2007), high sensitivity

We also conduct a second set of simulations from 1 January 2000 to 1 January 2001 to demonstrate the capability of the new module to simulate changes in plant productivity in response to changing CO<sub>2</sub> and subsequent changes in atmospheric chemistry. A half-year spin-up is conducted before the simulation period. The simulations are set up with only CO<sub>2</sub> being changed, while meteorological and other inputs remain unchanged. Table 2 summarizes the configuration of each simulation. Case 2a is the control experiment where prior configuration from the GEOS-Chem is used. Case 2b simulates the effect of elevated CO<sub>2</sub> on stomatal conductance by using the CO<sub>2</sub>-g<sub>s</sub> scaling factor described in Franks et al. (2013) (details are included in supplementary materials) and setting the ambient CO<sub>2</sub> concentration to 580 ppm, which is approximately the projected CO<sub>2</sub> concentration around 2050s in a business-as-usual scenario (e.g., Representative Concentration Pathway 8.5). This simple scaling approach has been suggested to investigate how rising CO<sub>2</sub> may affect ozone dry deposition in the future. This now allows us to compare between the mechanistic ecophysiology module, which simulates plant responses to rising CO<sub>2</sub> more mechanistically, and the semi-empirical CO<sub>2</sub>-g<sub>s</sub> scaling factor in the context of O<sub>3</sub> concentration and depositional sink. Cases 2c–f are conducted to compare the O<sub>3</sub> depositional sink and concentration to cases 2a–b, and to investigate how GPP and O<sub>3</sub> depositional sink changes under an elevated CO<sub>2</sub> scenario. Cases 2g–h are duplicates of 2c–d respectively, except that the isoprene emission rates are calculated using a photosynthesis-based scheme from Pacifico et al. (2011) instead of from the prior MEGAN emission inventory. They reveal whether the photosynthesis-based scheme yields a reasonable estimate of global isoprene emission under our model.

Deleted: the

Deleted: y

Deleted: new

Deleted: simple

Deleted: 2

470

**Table 2: Configuration of the second set of simulations that investigate gross primary productivity (GPP) and ozone (O<sub>3</sub>) concentration under an elevated CO<sub>2</sub> scenario.**

Case	[CO <sub>2</sub> ] (ppmv)	O <sub>3</sub> damage scheme and sensitivity	Stomatal conductance formulation	Isoprene emission
2a	370	No O <sub>3</sub> damage applied	Wesely (1989) parameterization and CO <sub>2</sub> scaling by Franks et al. (2013)	MEGAN v2.1
2b	580	No O <sub>3</sub> damage applied	Wesely (1989) parameterization and CO <sub>2</sub> scaling by Franks et al. (2013)	MEGAN v2.1
2c	370	No O <sub>3</sub> damage applied	Ecophysiology module	MEGAN v2.1
2d	370	Sitch et al. (2007), high sensitivity	Ecophysiology module	MEGAN v2.1
2e	580	No O <sub>3</sub> damage applied	Ecophysiology module	MEGAN v2.1
2f	580	Sitch et al. (2007), high sensitivity	Ecophysiology module	MEGAN v2.1
2g	370	No O <sub>3</sub> damage applied	Ecophysiology module	Photosynthesis-based scheme by Pacifico et al. (2011)
2h	370	Sitch et al. (2007), high sensitivity	Ecophysiology module	Photosynthesis-based scheme by Pacifico et al. (2011)

### 2.3 Evaluation data: SynFlux

480 We evaluate the modeled dry deposition velocity and concentration of O<sub>3</sub> against an observationally derived dataset known as Synthetic O<sub>3</sub> Flux (SynFlux) (Ducker et al., 2018). It derives site-level  $v_d$  by combining eddy covariance measurements of micrometeorological flux from FLUXNET sites in the United States and Europe with a gridded dataset of O<sub>3</sub> concentration. The aerodynamic and quasilinear sublayer resistances  $r_a$  and  $r_b$  from each of the sites are derived from the meteorological quantities measured at the sites. The surface conductance (reciprocal of resistance) is a summation of two

485 components: stomatal conductance  $g_s$  and non-stomatal conductance  $g_{ns}$ ;  $g_s$  is derived from the measured water vapor flux and meteorological data, and  $g_{ns}$  is estimated using Zhang et al. (2003). Figure 2 shows the locations of 36 SynFlux sites used in our evaluation of the ecophysiology module. [All sites with available data within the simulation interval are selected.](#) The total number of sites for each PFT is listed in the legend of Fig. 2. There are only two sites that represent C<sub>4</sub> grass, and they are ignored because observational data are only available in August. [The SynFlux dataset was evaluated at three sites with direct](#)

490 [O<sub>3</sub> flux measurements. The synthetic stomatal O<sub>3</sub> flux strongly correlates with measurements \( \$R^2 = 0.83-0.93\$ \) and the mean bias is modest \(21% or less\). In addition, 95% of the SynFlux values differ from measurements by less than a factor of two.](#)

The errors in SynFlux have been shown to be modest compared with differences between observations and regional and global CTMs that are frequently a factor of two or more, illustrating its utility for evaluating models (Ducker et al., 2018).

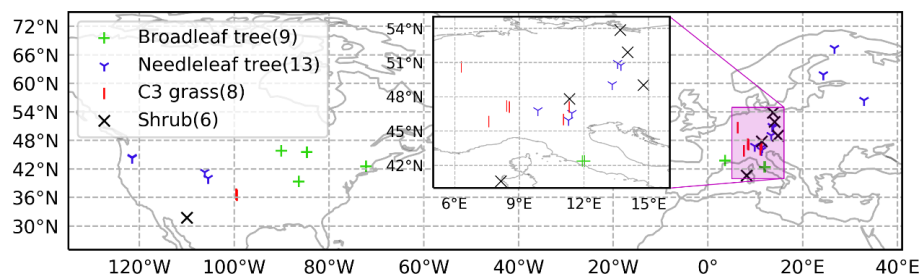


Figure 2: Locations of 36 SynFlux sites used in evaluation of the ecophysiology module. Different symbols indicate different plant functional types (PFTs) as broadleaf tree (Green “+”, includes evergreen broadleaf tree (EBF) and deciduous broadleaf tree (DBF)), needleleaf tree (Blue “Y”, includes evergreen needleleaf tree (ENF) only), C<sub>3</sub> grass (Red “|”, includes grassland (GRA) only), and shrub (Black “X”, includes wetland (WET), open shrubland (OSH) and closed shrubland (CSH)). Number of sites for each PFT is bracketed in the legend. Two C<sub>4</sub> grass (including savanna (SAV) and woody savanna (WSA)) sites are ignored in our evaluation due to a lack of observational data in our simulation period. Mixed forest (MF) and cropland (CRO) sites are not classified into any of the PFTs because they are usually composed of multiple PFTs.

### 3 Results

#### 3.1 Comparison between ecophysiology module and prior Wesely (1989) parameterization

We compare the modeled PFT-specific dry deposition velocity  $v_d$  and stomatal conductance  $g_s$  of O<sub>3</sub> in summer (JJA) to SynFlux. The modeled  $v_d$  and  $g_s$  were obtained by averaging hourly outputs from June to August 2012. They were then paired up with the SynFlux dataset by matching the month, location and PFT. In Fig. 3 and 4, the model results on model grid cells closest to the SynFlux sites are plotted against the corresponding observation-derived estimates from SynFlux for each PFT. C<sub>4</sub> grass is ignored due to a lack of observational data. The soil moisture stress factor  $\beta_t$  on the corresponding model grid is represented by the color of the circle.

Figure 3 shows that the ecophysiology module reduces the overestimation in  $v_d$  by the prior dry deposition module, especially for broadleaf trees, for which the root-mean-squared error (RMSE) decreases from 0.48 cm s<sup>-1</sup> to 0.11 cm s<sup>-1</sup>. C<sub>3</sub> grass shows a similar change where the RMSE decreases from 0.36 cm s<sup>-1</sup> to 0.21 cm s<sup>-1</sup> in case 1c (see Fig. S1), where high O<sub>3</sub> damage sensitivity is applied. C<sub>3</sub> grass is the most sensitive to O<sub>3</sub> damage among the four PFTs as the modeled  $v_d$  varies the most under different O<sub>3</sub> damage sensitivities. For needleleaf tree, the overestimation without the ecophysiology module becomes underestimation, regardless of the sensitivity of O<sub>3</sub> damage. O<sub>3</sub> damage barely affects  $v_d$ .

Deleted: was

Deleted: of  $v_d$

Deleted: It was

Deleted: T

Deleted: The lower  $v_d$  as simulated by the ecophysiology module is attributable to the ecophysiology-based stomatal conductance being generally smaller than that estimated by the semiempirical formulation, which was also discussed by Wong et al. (2019). The more significant decreases in  $v_d$  for broadleaf trees and needleleaf trees than for other PFTs are only due to the differences in formulations, but not due to any other physical reasons.

530

Figure 4 shows that the ecophysiology module significantly improves the simulation of  $g_s$  for broadleaf trees, needleleaf trees and shrubs, excluding those simulated with a soil moisture stress factor of  $\beta_f = 0$ . This exclusion is due to the assumption that the soil moisture stress parameterization is not well calibrated in the ecophysiology module. The results without the exclusion are available in Fig. S2. The RMSEs for both broadleaf trees and needleleaf trees decrease from 0.90 and 0.75  $\text{cm s}^{-1}$  to 0.15 and 0.21  $\text{cm s}^{-1}$ , respectively. For shrubs, the RMSE also decreases from 0.50 to 0.03–0.04  $\text{cm s}^{-1}$  (depending on sensitivity of  $\text{O}_3$  damage applied, see Fig. S2). For  $\text{C}_3$  grass, the mechanistic formulation slightly decreases  $g_s$ , which is consistent with the results in Fig. 3. Combining the validation of  $v_d$  and  $g_s$ , we find that the lower  $v_d$  as simulated by the ecophysiology module is attributable to photosynthesis-based stomatal conductance being generally smaller than that estimated by the semiempirical formulation, which was also discussed by Wong et al. (2019).

535

Deleted: under

Deleted: an

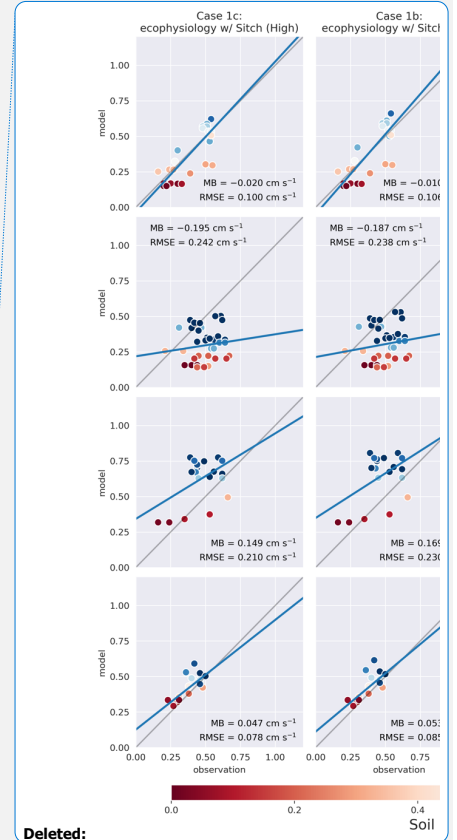
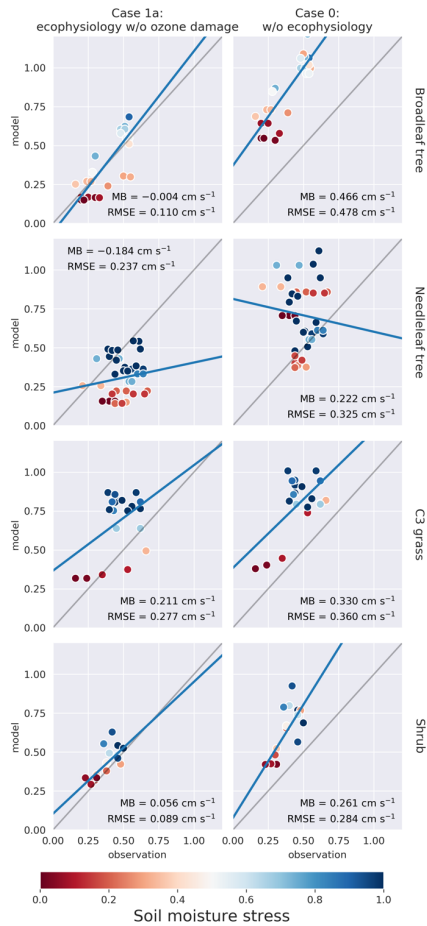
Deleted: such assumption

Deleted: drastically

Deleted:

Deleted: the ecophysiology

Deleted: ¶



Deleted:

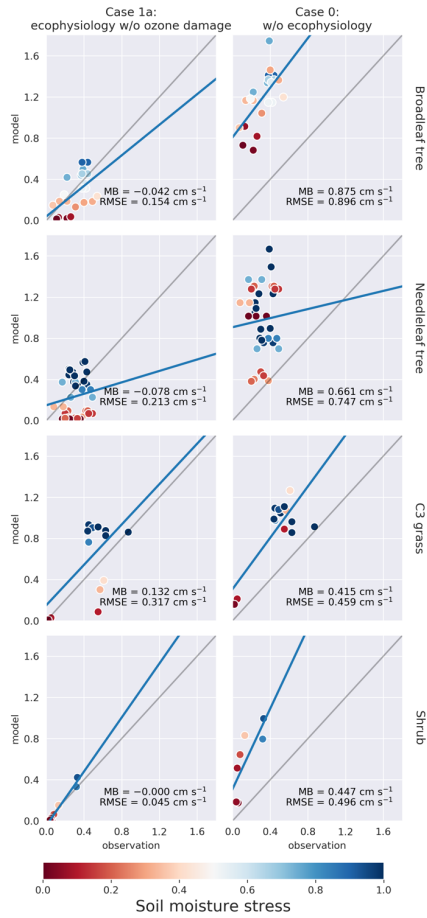
Deleted: ,

Deleted: , 1b and 1c.

545

Figure 3: Plots of modeled monthly mean dry deposition velocity of  $O_3$  ( $cm s^{-1}$ ) in northern summer (JJA) against SynFlux estimates, categorized by site PFT for each simulation case. Columns from right to left represent simulation cases 0 and 1a respectively. Each row corresponds to a PFT.  $C_4$  grass is ignored due to a lack of observational data. The soil moisture stress factor  $\beta_t$  on the corresponding model grid cell is represented by the color of the circle. Mean bias (MB) and root-mean-squared error (RMSE) are shown for each plot. [Full results including cases 1b and 1c can be found in the supplementary materials.](#)

550



555 **Figure 4:** Same as Fig. 3 but for monthly mean stomatal conductance  $g_s$  ( $\text{cm s}^{-1}$ ) under  $\beta_i \neq 0$  condition. For results including  $\beta_i = 0$  condition, please refer to Fig. S2.

In Fig. 3–5, the colors of circles represent the soil moisture stress factor  $\beta_i$  described in Sect. 2.1.5. In the semi-empirical parameterization,  $v_a$  and  $g_s$  do not depend on  $\beta_i$ . However,  $v_a$  and  $g_s$  simulated using the ecophysiology module are

**Deleted:** Since the stomatal resistance

**Deleted:** es

**Deleted:** in the semi-empirical parameterization,  $v_a$  also does not correlate with  $\beta_i$

**Deleted:** is

565 significantly affected by  $\beta_t$  as  $v_d$  and  $g_s$ , with low  $\beta_t$  are almost always lower than those with high  $\beta_t$ , regardless of site locations. Also, for broadleaf trees and needleleaf trees, low  $\beta_t$  values appear to result in a nearly constant value of  $v_d = 0.2 \text{ cm s}^{-1}$ , reflecting mostly non-stomatal deposition, while high  $\beta_t$  gives a much closer estimate of  $g_s$  and  $v_d$  to observations. Since  $g_s$  is multiplied by  $\beta_t$  as described in Sect. 2.1.5, low  $\beta_t$  values should indeed give lower  $g_s$  and thus lower  $v_d$ . At different site locations, other components of  $v_d$  can also vary, but the strong correlation between  $\beta_t$  and  $v_d$  remains. Whether  $v_d$  is sensitive to vapor pressure deficit (VPD) in a similar fashion arguably warrants further investigation. Overall, our results indicate that  $\beta_t$  is an important parameter in this formulation and strongly affects the model performance on simulating dry deposition velocity. However, there is a large inter-model variation in  $\beta_t$  due to variability in soil moisture, different formulations of  $\beta_t$  and vertical resolution of soil levels (Trugman et al., 2018). Since GEOS-Chem does not simulate soil explicitly, we only use a simple and empirical parameterization of  $\beta_t$  with input of a single-layer soil moisture from the MERRA-2 dataset. Such deficiency in the representation of  $\beta_t$  may render the model less reliable in simulating the potential impact of drought events on atmospheric chemistry and plant productivity. Therefore, simulation of drought events, which is one of the potential uses of the ecophysiology module, should be interpreted cautiously unless parameters in the  $\beta_t$  function are more thoroughly calibrated on a regional or local basis. Despite the uncertainty of  $\beta_t$ , we emphasize that including the stomatal responses to VPD and soil moisture is valuable because the Wesely (1989) parameterization cannot represent such stomatal responses. We also compare the model results of monthly mean  $\text{O}_3$  concentration in summer with SynFlux estimates, derived from a gridded dataset of  $\text{O}_3$  concentration. Figure S<sub>4</sub> shows the comparison of monthly mean  $\text{O}_3$  concentration on model grid cells closest to the SynFlux sites against the corresponding estimates from SynFlux categorized by site PFT. According to the rightmost column,  $\text{O}_3$  concentration is originally overestimated by the GEOS-Chem model. The ecophysiology module increases the model bias by 4 to 5 ppbv for broadleaf trees, needleleaf trees and C<sub>3</sub> grasses, and 2 ppbv for shrubs. Activation of the  $\text{O}_3$  damage scheme and the change of sensitivity to  $\text{O}_3$  damage only produce modest differences (see Fig. S3) in terms of monthly mean  $\text{O}_3$  concentration, representing relatively weak  $\text{O}_3$ -vegetation feedback effects.

585 There can be multiple possible reasons leading to the biases in  $\text{O}_3$  concentration. First, the simulated  $\text{O}_3$  concentration on nearby model grid cells is only a bulk average over the entire area of the grid cell, while the measurement reflects the local  $\text{O}_3$  concentration. Subgrid variability created by local meteorology or surface topography is not accounted for during the comparison. Unlike dry deposition velocity, it is not possible to separate  $\text{O}_3$  concentration into PFT-specific quantity for a fair comparison. Secondly, accurate simulation of  $\text{O}_3$  relies on many non-stomatal depositional and non-depositional processes as well, e.g., chemistry, photochemistry, emissions of precursor gases, etc. Since we show that simulation of dry deposition velocity of  $\text{O}_3$  is improved by the ecophysiology module, modifications in non-stomatal depositional and non-depositional processes would be required more urgently to improve the performance in  $\text{O}_3$  simulations. The problems of general overestimation of  $\text{O}_3$  by various models at northern midlatitudes have been discussed by Travis et al. (2016).

595

Deleted: 1

Deleted: 4



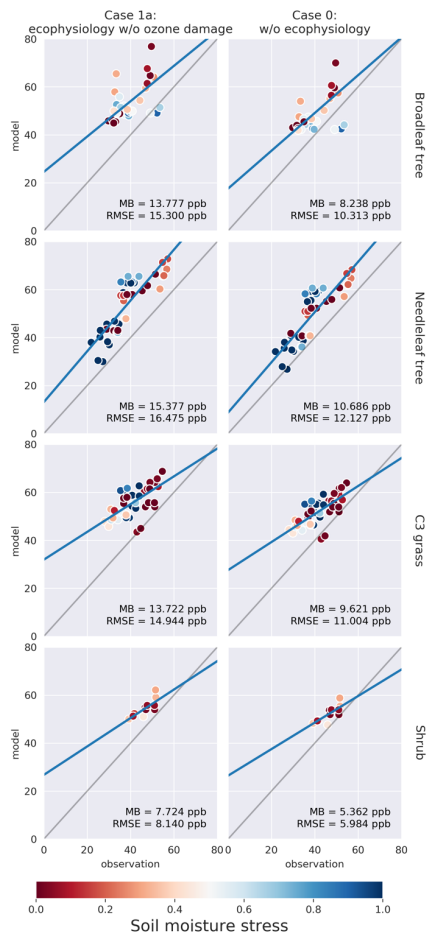
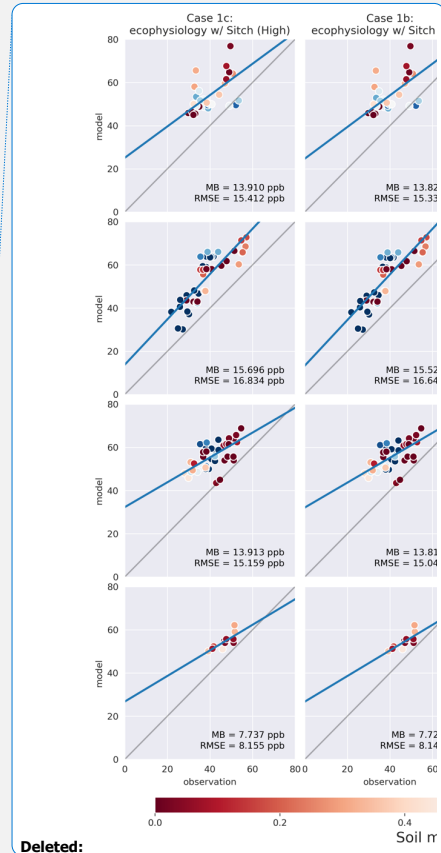


Figure 5: Same as Fig. 3, but for modeled monthly mean O<sub>3</sub> concentration (ppbv).



Deleted:

Deleted: Plots of modeled monthly mean O<sub>3</sub> concentration (ppbv) in northern summer (JJA) against SynFlux data, categorized by site PFT for each simulation case. Columns from right to left represent simulation cases 0, 1a, 1b and 1c. Each row corresponds to a PFT. C<sub>3</sub> grass is ignored due to a lack of observational data. The soil moisture stress factor  $\beta_t$  on the corresponding model grid cell is represented by the color of the circle. Mean bias (MB) and root-mean-squared error (RMSE) is shown for each plot....

### 3.2 GPP and O<sub>3</sub> depositional sink simulated by the ecophysiology module under different CO<sub>2</sub> levels

615 In the second set of simulations, we demonstrate that with the new dynamic linkage to ecophysiology, the model is  
 620 capable of capturing CO<sub>2</sub>-O<sub>3</sub>-vegetation interactions under elevated CO<sub>2</sub> concentration. Table 3 tabulates the global GPP and  
 the O<sub>3</sub> depositional sink for each of the cases, and Fig. 6 shows their spatial distributions. Under the year 2000-level CO<sub>2</sub>  
 scenario, the simulated gross primary production (GPP) is 119 Pg C yr<sup>-1</sup> and the total O<sub>3</sub> depositional sink is 772 Tg O<sub>3</sub> yr<sup>-1</sup>  
 in the absence of O<sub>3</sub> damage. The global O<sub>3</sub> deposition flux is close to the mean value from 12 CTMs (747 Tg O<sub>3</sub> yr<sup>-1</sup>) used  
 in the Third Assessment Report of the Intergovernmental Panel on Climate Change (IPCC TAR) (Prather and Ehhalt, 2001),  
 but is generally lower than the values from later multi-model studies, e.g., 1003 ± 200 Tg O<sub>3</sub> yr<sup>-1</sup> from Stevenson et al. (2006)  
 and 902 ± 255 Tg O<sub>3</sub> yr<sup>-1</sup> from Wild (2007). A possible reason is that most CTMs use a semi-empirical formulation of the  
 stomatal conductance, which is generally larger than ecophysiology-based stomatal conductance (Wong et al., 2019), and thus  
 higher dry deposition fluxes in other CTMs are expected. Globally, the O<sub>3</sub> damage on GPP is 4.2 Pg C yr<sup>-1</sup> (3.5%), but the O<sub>3</sub>  
 damage percentage can reach more than 20% regionally, for example in China, as shown in Fig. 6c.

Deleted: ure

Deleted: 5

Deleted: (

Deleted: Stevenson et al., 2006; Wild, 2007

Deleted: (mean ± s.d.)

Deleted: ;

Deleted: ; Young et al., 2018

Deleted: )

Deleted: 4

**Table 3: Annual global GPP and total O<sub>3</sub> depositional sink in each simulation.**

Case	Global GPP (Pg C yr <sup>-1</sup> )	O <sub>3</sub> depositional sink (Tg O <sub>3</sub> yr <sup>-1</sup> )	<u>Elevated</u> <u>CO<sub>2</sub></u>	<u>Ecophysiology</u> <u>module</u>	<u>O<sub>3</sub> dam-</u> <u>age</u>	<u>E<sub>isoprene</sub> depends</u> <u>on A<sub>c</sub>?</u>
2a	N/A	863.6	<u>No</u>	<u>No</u>	<u>N/A</u>	<u>N/A</u>
2b	N/A	812.9	<u>Yes</u>	<u>No</u>	<u>N/A</u>	<u>N/A</u>
2c	119.0	772.1	<u>No</u>	<u>Yes</u>	<u>No</u>	<u>No</u>
2d	114.8	768.1	<u>No</u>	<u>Yes</u>	<u>Yes</u>	<u>No</u>
2e	138.6	746.3	<u>Yes</u>	<u>Yes</u>	<u>No</u>	<u>No</u>
2f	136.0	744.5	<u>Yes</u>	<u>Yes</u>	<u>Yes</u>	<u>No</u>
2g	119.4	766.4	<u>No</u>	<u>Yes</u>	<u>No</u>	<u>Yes</u>
2h	115.3	761.3	<u>No</u>	<u>Yes</u>	<u>Yes</u>	<u>Yes</u>

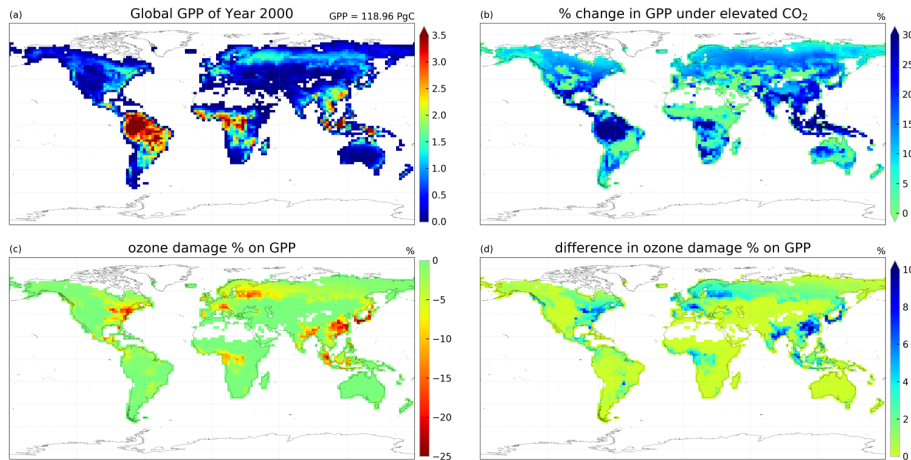


Figure 6a–d: Maps of (a) global GPP distribution ( $\text{kg C m}^{-2} \text{yr}^{-1}$ ) in case 2c, (b) percentage change in GPP driven by  $\text{CO}_2$  concentration increase, (c) percentage change in GPP driven by high-sensitivity  $\text{O}_3$  damage, and (d) difference in  $\text{O}_3$ -driven percentage change in GPP between experiments with year-2000 and elevated  $\text{CO}_2$  concentrations, where the positive values indicate a reduction in ozone damage.

640

Deleted: 5

Under elevated  $\text{CO}_2$  scenario (case 2e minus 2c), GPP is projected to increase by  $19.7 \text{ Pg C yr}^{-1}$  (16.8%) globally, and up to 30% regionally near tropics (Fig. 6b). We note also that such changes in GPP are entirely due to higher photosynthetic rate, since LAI is prescribed. The global  $\text{O}_3$  depositional flux decreases by  $25.8 \text{ Tg O}_3 \text{ yr}^{-1}$  (3.3%). This change is about half of that given by the  $\text{CO}_2$ - $g_s$  scaling factor experiments (cases 2b minus 2a) implying that, compared to the simple  $\text{CO}_2$ - $g_s$  scaling factor, the mechanistic ecophysiology module predicts less reduction in stomatal conductance at a higher  $\text{CO}_2$  level. It should be noted that the semi-empirical  $\text{CO}_2$ - $g_s$  scaling factor is an approximation based only on the RuBP-limited photosynthesis rate (Franks et al., 2013), thus does not necessarily represent the full range of limiting or compensating conditions for photosynthesis. The magnitude of  $\text{O}_3$  percentage damage is reduced by around 10 percentage points (i.e., the percentage damage goes from about -20% to -10%) in regions with originally high  $\text{O}_3$  damage such as southern China, Europe and the eastern US (Fig. 6d). The monthly distribution of GPP also generally agrees with results from other models. Figure 7a shows the monthly distribution of global GPP and Fig. 7b–f show the area-weighted average GPP for each of the PFTs. Our results demonstrate a seasonal cycle of GPP that peaks at around  $130 \text{ g C m}^{-2} \text{ month}^{-1}$  in July and falls steadily to around  $60 \text{ g C m}^{-2} \text{ month}^{-1}$  in February. This resembles with observation-derived datasets like FLUXNET-MTE, as shown in Fig. 3a of Slevin et al. (2017). When the seasonal cycle of GPP for each PFT is considered separately, different trends and features are present.

645

Deleted: 5

Deleted: is

Deleted: and no changes in LAI are simulated

650

Deleted: simple

Deleted: %

655

Deleted: 5

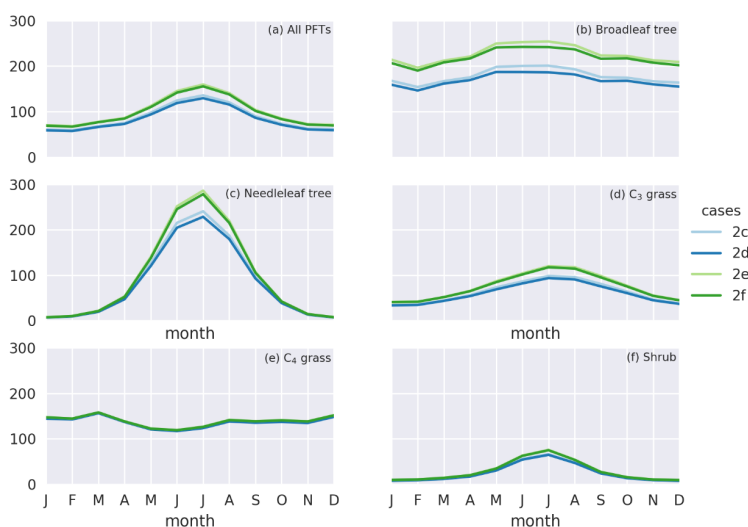
Deleted: To conclude, it is shown that the model can capture both the direct  $\text{CO}_2$  fertilization effect on GPP and the mitigation of  $\text{O}_3$  damage under elevated  $\text{CO}_2$ , leading to higher GPP via both pathways.

Deleted: 6

Deleted: 6

670 For broadleaf trees, the average GPP stays around 150 to 200  $\text{g C m}^{-2} \text{ month}^{-1}$  throughout a year and is slightly higher in northern summer.  $\text{C}_4$  grasses also have a steady average GPP of around 100 to 150  $\text{g C m}^{-2} \text{ month}^{-1}$  but have an opposite cycle to all other PFTs. For needleleaf trees,  $\text{C}_3$  grasses and shrubs, GPP is very low in northern winter, but for needleleaf trees, it rises to more than 200  $\text{g C m}^{-2} \text{ day}^{-1}$  in July, which is the highest among all PFTs. Under the elevated  $\text{CO}_2$  scenario, GPP is projected to rise by 10 to 30  $\text{g C m}^{-2} \text{ month}^{-1}$ , higher in northern summer and vice versa. Most of the increase in GPP can be attributed to broadleaf trees and needleleaf trees, which have larger total leaf surface area than grasses and shrubs, thus amplifying the enhanced photosynthesis under higher ambient  $\text{CO}_2$  concentration, as suggested by Eq. (S8) in [the supplementary materials](#). On the other hand,  $\text{C}_4$  grasses show no change in average GPP throughout a year.

Deleted: Sect. 2.1.3



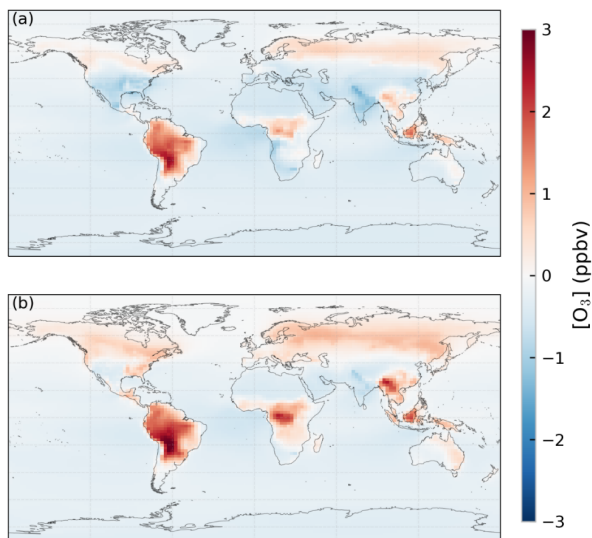
680 **Figure 7a–f:** Monthly gross primary productivity (GPP) ( $\text{g C m}^{-2} \text{ month}^{-1}$ ) for simulation cases 2c–f for (a) all PFTs, (b) broadleaf trees, (c) needleleaf trees, (d)  $\text{C}_3$  grasses, (e)  $\text{C}_4$  grasses and (f) shrubs. Blue and green lines denote simulation cases under year-2000 and elevated  $\text{CO}_2$  level respectively. Darker and paler lines denote cases with and without  $\text{O}_3$  damage, respectively.

Deleted: 6

685  $\text{O}_3$  concentration only changes moderately under elevated  $\text{CO}_2$  concentration overall, but with larger changes happening in some regions. Figure 8 shows the change in annual mean  $\text{O}_3$  concentration under the increase in  $\text{CO}_2$  concentration for cases 2b and 2e. In addition to larger increases of up to 3 ppbv found in the Amazon forest and Borneo regions, smaller increases of up to 1 ppbv are also found in central Africa, Southeast Asia and at middle-high latitudes. This agrees with the

Deleted: 7

simulation result using the CO<sub>2</sub>-g<sub>s</sub> scaling factor (case 2b). The latter shows even stronger increases in O<sub>3</sub> concentration over the Amazon forest, central Africa and Southeast Asia.



695 Figure 8a–b: Changes in ozone (O<sub>3</sub>) concentration (ppbv) due to the increase in CO<sub>2</sub> concentration simulated using (a) the ecophysiology module and (b) the CO<sub>2</sub>-g<sub>s</sub> scaling factor.

Deleted: 7

### 3.3 Comparison of isoprene emission rates between photosynthesis-dependent formulation and MEGAN v2.1 emission model

700 Implementing a photosynthesis-dependent isoprene emission scheme into the GEOS-Chem introduces another interaction between ecophysiology and atmospheric chemistry. Here, we demonstrate that the simulated isoprene emission rates are close to what the MEGAN emission algorithm simulates. The annual isoprene emission rates in year 2000 using the MEGAN emission inventory (case 2c) and the photosynthesis-dependent scheme from Pacifico et al. (2011) (case 2g) are shown in Fig. 9a–b, and the annual totals are 349.1 Tg C and 317.9 Tg C respectively. The annual isoprene emission totals are at the lower end of other published estimates of 300–530 Tg C (as summarized in Table 3 in Weng et al., 2020), but are consistent with Weng et al. (2020), who estimated 330–345 Tg C yr<sup>-1</sup> using the MEGAN v2.1 at a finer spatial resolution than this study.

Deleted: 8

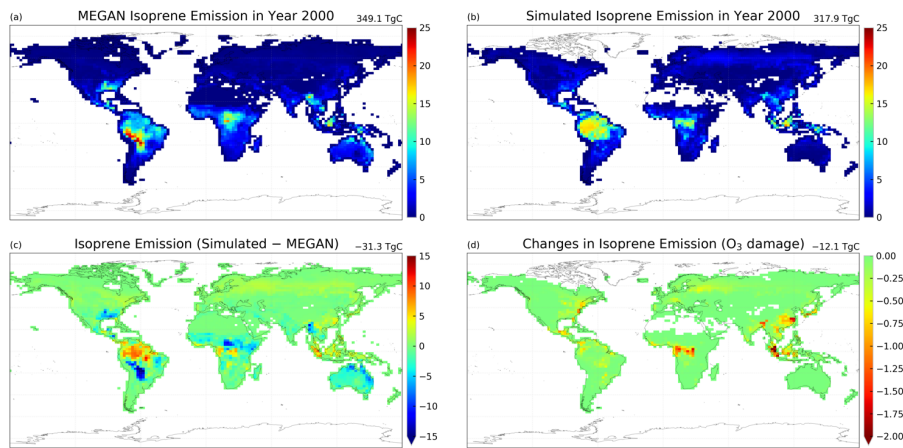
Deleted: HEMCO

710 The monthly averages of land surface temperature in year 2000 are lower than the 2000–2009 monthly averages (See Fig. S4),  
 which can lower the emission total. The simulated isoprene emission rate is similar to the MEGAN emission model in general,  
 as the tropics, especially the Amazon forest, contributes the most to the annual isoprene emission total. There are, however,  
 some modest differences in the magnitude and location of the largest emission flux in each of the continents, e.g., from  $-15$  to  
 $+10 \text{ g C m}^{-2} \text{ yr}^{-1}$  in different parts of South America, and about  $-5 \text{ g C m}^{-2} \text{ yr}^{-1}$  in the southern US and Australia. Since the  
 715 isoprene emission rate is proportional to the photosynthesis rate as in Eq. (9), these differences can be due to the simple  
 classification of PFTs, which can constraint the maximum photosynthesis capacity and thus the photosynthesis rate. We also  
 note that the MEGAN emission model is also subject to uncertainties in its algorithm. Besides, temperature variability in the  
 subgrid scale is often a major source of uncertainty, since a temperature difference of  $+1^\circ\text{C}$  is equivalent to a  $+10\%$  increase  
 in isoprene emission rate, as inferred from Eq. (S17). Figure 9d shows that global isoprene emission decreases by  $12.1 \text{ Tg C}$   
 720  $\text{yr}^{-1}$  (3.8%) (case 2h minus 2g) due to  $\text{O}_3$  damage on vegetation. This reduction is mainly due to the 3.5% decrease in GPP via  
 the dry deposition pathway, as described in Sect. 3.2.

Deleted: 1

Deleted: 16

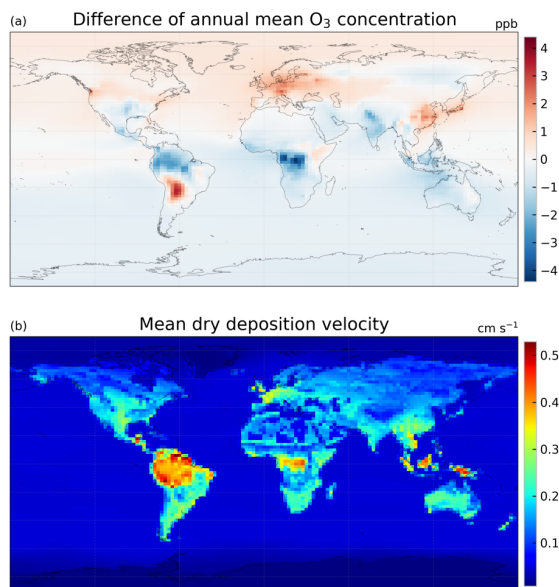
Deleted: 8



725 Figure 9a–d: Annual mean isoprene emission rates ( $\text{g C m}^{-2} \text{ yr}^{-1}$ ) for year 2000 simulated using (a) the MEGAN emission model  
 (case 2c) and (b) the Pacifico et al. (2011) scheme coupled with the ecophysiology module without  $\text{O}_3$  damage (case 2g), and the  
 differences in mean isoprene emission rates due to (c) switching emission schemes (case 2g minus 2c) and (d)  $\text{O}_3$  damage on photo-  
 synthesis, which is proportional to isoprene emission rates (case 2h minus 2g). The number on the top right corner denotes the area-  
 weighted total of emitted isoprene. White color in the figures denotes zero value.

Deleted: 8

In terms of GPP and O<sub>3</sub> depositional sink, switching isoprene emission scheme from the MEGAN emission model to a photosynthesis-based scheme by Pacifico et al. (2011), i.e., comparing case 2c to case 2g, does not change the GPP when O<sub>3</sub> damage is absent, as shown in Table 3. This is expected because turning off the O<sub>3</sub> damage scheme would interrupt the feedback pathways as shown in Fig. 1, so vegetation productivity would not be affected by atmospheric chemistry. The O<sub>3</sub> depositional sink is however affected because isoprene is a precursor gas of O<sub>3</sub>. It is lowered by 5.7 Tg O<sub>3</sub> yr<sup>-1</sup> (0.74%), due to a lower mean O<sub>3</sub> concentration in the tropics (Fig. 10a) where the dry deposition velocity is generally higher (Fig. 10b). The reduction in GPP due to O<sub>3</sub> damage does not differ as the isoprene emission scheme changes, as inferred by comparing cases 2c–d to 2g–h. This is likely due to the changes of O<sub>3</sub> concentration being too small to cause a significant feedback effect. Additional experiments would be required to quantify the feedback effect via the isoprene emission pathway.



745 **Figure 10a–b:** (a) Difference in annual mean O<sub>3</sub> concentration (ppbv) between using the MEGAN emission model and the Pacifico et al. (2011) photosynthesis-based isoprene emission scheme (case 2g minus 2c) and (b) annual mean dry deposition velocity of O<sub>3</sub> (cm s<sup>-1</sup>) simulated with the ecophysiology module (case 2g, and it should be very similar to case 2c).

Deleted: 9

Deleted: 9

Deleted: 9

#### 4 Conclusions and discussion

Ecophysiology-based approaches in modelling  $g_s$  allow models to capture changes in plant stomatal and emission behaviors, which are essential in simulating biosphere–atmosphere exchange of gaseous species and  $O_3$ –vegetation interactions. In this study, we incorporate an ecophysiology module into the GEOS-Chem CTM to couple changes in atmospheric chemistry to changes in plant ecophysiological behaviors mechanistically, [enabling the model to address how vegetation responses to climatic changes may modify atmospheric chemistry and capture two specific  \$O\_3\$ –vegetation feedback pathways as shown in Fig. 1: \(1\) reduced photosynthesis due to plant stomatal  \$O\_3\$  uptake suppresses isoprene emission, which modulates the formation of  \$O\_3\$ ; \(2\)  \$O\_3\$  damage on plants reduces stomatal conductance and thus  \$O\_3\$  dry deposition, leading to higher surface  \$O\_3\$  concentration](#). We then validate the simulated dry depositional velocity, [stomatal conductance](#) and concentration of  $O_3$  against SynFlux, which is an observation-derived dataset that constrains  $O_3$  deposition from measured water, heat, and momentum fluxes. Moreover, the module can also simulate canopy photosynthesis, which is also used for calculating isoprene emission and  $O_3$ –vegetation interactions and is itself an important indicator for ecosystem productivity and health. We investigate  $O_3$  deposition flux and GPP under present-day and elevated  $CO_2$  concentrations. This module provides a unique ability in evaluating the effects of pollutant deposition on air quality and plant health by allowing plant physiology to respond dynamically to changes in atmospheric chemistry and meteorological conditions.

By using a mechanistic, photosynthesis-based representation of  $g_s$  instead of the semi-empirical parameterization of Wesely (1989), the ecophysiology module [significantly reduces the overestimation of  \$g\_s\$  by up to  \$0.7 \text{ cm s}^{-1}\$  and thus](#) reduces the overestimation in dry deposition velocity  $v_d$  of  $O_3$  in northern summer by  $0.1$ – $0.3 \text{ cm s}^{-1}$  across different PFTs when compared to the SynFlux observation-based dataset. The reduction is the largest for broadleaf trees and  $C_3$  grasses. Lei et al. (2020), who coupled an integrated biosphere model to GEOS-Chem, showed that the change in annual mean  $v_d$  of  $O_3$  due to a coupled stomatal conductance is only up to  $-0.15 \text{ cm s}^{-1}$ . However, the reduction in  $v_d$  is not uniform in all seasons, but generally larger in summer, as shown in their seasonal cycle of  $v_d$ . When the comparison is restricted to the same season, our results agree with Lei et al. (2020). We further highlight that values of  $v_d$  are heavily affected by the soil moisture stress factor  $\beta_t$ . Representation of  $\beta_t$  is not very reliable in the current generation of models, and thus this is one of the [limitations of our studies](#). More thorough calibration of parameters related to soil water stress to more localized observations over higher spatiotemporal resolutions, as well as consideration of more soil moisture layers and distribution specific to PFTs or regions, is recommended. [Here we emphasize that introducing a mechanistic representation of  \$g\_s\$  into GEOS-Chem is valuable because the Wesely \(1989\) parameterization cannot represent stomatal responses to vapor pressure deficit and soil moisture, which is an essential step toward studying the influence of climatic stresses such as droughts and heatwaves on the interactions between atmospheric chemistry and vegetation](#).

Due to a decrease in dry deposition velocity of  $O_3$ , simulated  $O_3$  concentration increases by 2–5 ppbv, amplifying the original overestimation by GEOS-Chem. Lei et al. (2020) also showed similar magnitude of changes (1–3 ppbv) in terms of

**Deleted:** Tropospheric  $O_3$  is a major air pollutant that is harmful to vegetation. It is altered by vegetation through dry deposition on plant surface and emission of BVOCs. Dry deposition to plant stomata is mainly controlled by the bulk canopy stomatal conductance  $g_s$ , which represents the openness of plant stomata in a canopy.  $g_s$  is regulated by plant physiological processes such as photosynthesis and transpiration, and thus varies strongly with environmental conditions. Moreover, plant stomata can be damaged upon exposure to  $O_3$ , resulting in reduced  $g_s$ . However, such variability is often not fully captured in CTMs. For example, the response of  $g_s$  to atmospheric or soil moisture content is missing in some models.  $CO_2$  and  $O_3$  concentrations also modify stomatal behavior, and in turn affect air pollutant concentrations. Therefore, e

**Deleted:** have been suggested. They

**Deleted:** First, reduced photosynthesis due to plant stomatal  $O_3$  uptake suppresses the emission of isoprene, which modulates the formation of  $O_3$ ; Second,  $O_3$  damage on plants reduces stomatal conductance and thus the dry deposition flux of  $O_3$ , leading to higher surface  $O_3$  concentration

**Deleted:** main sources of uncertainties in our results

**Deleted:** However,

**Deleted:** which is an essential step towards studying the effects of pollutant deposition on plant health under the influence of other stresses such as droughts and heatwaves



annual surface O<sub>3</sub> concentration, and attributed the increase in O<sub>3</sub> concentration mostly to changes in v<sub>d</sub>. Given the improvements in model performance for [stomatal conductance and dry deposition velocity](#) per se, the worsened overestimation of O<sub>3</sub> concentration [calls for improvements and modifications of non-stomatal depositional and non-depositional processes in CTMs.](#)

Deleted: implies greater urgency for the

810 We also demonstrate that the ecophysiology module is capable of simulating O<sub>3</sub> deposition, plant productivity and O<sub>3</sub>-vegetation interactions under year-2000 CO<sub>2</sub> (370 ppm) and elevated CO<sub>2</sub> (580 ppm) scenarios. Under the present-day CO<sub>2</sub> scenario, the global annual GPP [without O<sub>3</sub> damage](#) is 119 Pg C yr<sup>-1</sup>. The reduction in GPP due to O<sub>3</sub> damage is 4.2 Pg C yr<sup>-1</sup> (3.5%) globally, and the percentage reduction can be more than 20% in the eastern US and China. This percentage roughly agrees with [an estimate of 2–5% by Yue and Unger \(2015\)](#), who applied the same O<sub>3</sub> damage scheme from Sithich et al. (2007) to estimate global changes in GPP. An elevated CO<sub>2</sub> concentration leads to higher GPP through both direct CO<sub>2</sub> fertilization effect (+19.7 Pg C yr<sup>-1</sup>) and mitigation of O<sub>3</sub> damage (+1.5 Pg C yr<sup>-1</sup>). Monthly GPP distribution generally agrees with other models. The global O<sub>3</sub> deposition flux simulated under year-2000 CO<sub>2</sub> concentration is 772 Tg O<sub>3</sub> yr<sup>-1</sup>, which is low relative to some multi-CTM studies, e.g., [1003 ± 200 Tg O<sub>3</sub> yr<sup>-1</sup> from Stevenson et al., \(2006\) and 902 ± 255 Tg O<sub>3</sub> yr<sup>-1</sup> from Wild, \(2007\)](#). This is mostly attributable to the semi-empirical stomatal conductance used in other CTMs being generally 820 larger than the ecophysiology-based stomatal conductance, resulting in a larger deposition flux. [Estimates of global O<sub>3</sub> deposition flux can also differ due to other factors such as oceanic deposition \(Pound et al., 2020\)](#). We also compare calculating g<sub>s</sub> with the [mechanistic](#) ecophysiology formulations to using the [semi-empirical](#) CO<sub>2</sub>-g<sub>s</sub> scaling factor suggested by Franks et al. (2013) in terms of O<sub>3</sub> deposition flux. The decrease in global O<sub>3</sub> deposition flux due to an elevated CO<sub>2</sub> concentration using the ecophysiology module is almost half of that using the CO<sub>2</sub>-g<sub>s</sub> scaling factor based on light-limited photosynthesis rate, 825 implying that such a simple scaling approach may substantially overestimate the effect of elevated CO<sub>2</sub> on stomatal conductance and thus O<sub>3</sub> deposition.

Deleted: (

Deleted: ,

Deleted: ;

Deleted: ,

We also implement a photosynthesis-based isoprene emission scheme in the ecophysiology module. The simulated global isoprene emission total is 317.9 Tg C yr<sup>-1</sup>, which is 31.3 Tg C yr<sup>-1</sup> (-9.0%) less than the values calculated using the MEGAN emission model in GEOS-Chem. The commonly accepted range is around 300–500 Tg C yr<sup>-1</sup> and the simulated 830 value is on the lower end of this range. The variability of model estimates can arise from different algorithms, vegetation presentation and other input data sources. A recent study by Weng et al. (2020) estimated a narrower range of 330–345 Tg C yr<sup>-1</sup> particularly for [MEGAN v2.1](#), which is included as the emission component of the GEOS-Chem model. Our simulated value for global isoprene emission total using the Pacifico et al. (2011) scheme is comparable. The reduction in isoprene emission due to the O<sub>3</sub> damage on GPP is 12.1 Tg C yr<sup>-1</sup> (-3.8%), which is mainly attributable to the dry deposition pathway. 835 All in all, the implementation of the new scheme not only serves as an alternative of the MEGAN emission model to simulate isoprene emission, but also brings new research opportunities that require isoprene emission to be mechanistically linked to plant physiology.

Deleted: HEMCO

845 Limitations exist within our study. Our module only simulates ecophysiological processes directly related to photo-  
synthesis. Unlike Lei et al. (2020), who coupled a CTM to an integrated biosphere model, we do not simulate any biogeo-  
chemical processes and ecosystem structural changes such as carbon allocation, long-term growth in biomass, litter, or soil  
decomposition. In particular, LAI does not change dynamically with climatic conditions or O<sub>3</sub> damage in the current model.  
This, however, allows our module to be computationally more efficient and perform better with respect to the reproduction of  
observations, when compared to other models that simulate a larger array of processes of terrestrial ecosystems extensively.  
850 The difference in computational speed from the prior GEOS-Chem v12.2.0 is barely noticeable (< 20% increase in dry depo-  
sition module run time, and < 0.001% increase in total model run time for a 6-month simulation). There are also fewer relevant  
ecophysiological factors contributing to variabilities in atmospheric chemistry. Thus, our module should be preferred over  
fully coupled Earth system models or coupling a CTM with a biosphere model (e.g., Lei et al. (2020)) if short-term (seasonal  
or interannual) atmosphere–biosphere exchange and air quality responses to intermittent meteorological events and stressors  
855 with a given ecosystem structure and distribution are concerned. ~~We can also examine such interactions with a prescribed,  
hypothetical land cover according to future land use scenarios or in response to future climatic changes as simulated by any  
biogeochemical models.~~ In contrast, if long-term (e.g., multi-decadal and multi-centurial) dynamic evolution of ecosystem  
structure and distribution, e.g., in response to higher CO<sub>2</sub> level, climate change or nitrogen deposition, is an essential aspect of  
the study, the coupled modeling framework may be preferred.

860 ~~Uncertainties in soil moisture and water stress also represent an important limitation to our model for arid and semiarid  
environments. The simulated  $g_s$  and  $v_d$  are heavily affected by a linearly parameterized function known as the soil moisture  
stress factor  $\beta_s$ , which is a common approach in vegetation models (Powell et al., 2013). It is worth noting that soil moisture  
could be a highly variable quantity in different models, because of different vertical resolution of the soil layers, and the  
dependence on other model-specific quantities such as porosity and hydraulic conductivity (Dirmeier et al., 2006; Koster et  
865 al., 2009). There have been several studies (Blyth et al., 2011; Verhoef and Egea, 2014; Harper et al., 2021) on improving the  
representation of soil moisture stress in the Joint UK Land Environmental Simulator (JULES), from which we adopted the  
formulations. The development of the ecophysiology module in this study serves as a first and essential step toward represent-  
ing interactions between atmospheric chemistry and plant ecophysiology in a CTM; improving the representation of soil mois-  
ture stress and calibrating it with respect to specific locations and events will be an important and promising future application  
870 of such a model.~~

~~Uncertainties in the SynFlux dataset for model evaluation should also be noted. The dataset was itself only evaluated  
at three sites with direct O<sub>3</sub> flux measurements, but Ducker et al. (2018) showed that the synthetic stomatal O<sub>3</sub> flux strongly  
correlates with measurements and the mean bias is modest, and assumed that the uncertainties at other sites would not differ  
significantly. Comparing coarse-resolution model results with point measurements as in SynFlux could also be problematic  
875 due to subgrid variability. However, they showed that 95% of the SynFlux values differ from measurements by less than a~~

Deleted:

Deleted: s

Deleted: s

Deleted: results

Deleted: also

Deleted: from

Deleted: s

Deleted: GEOS-Chem

Deleted: , and improving representation of soil moisture stress can be listed as one of the future directions

Deleted: is

Deleted: ( $R^2 = 0.83-0.93$ )

Deleted: (21% or less)

Deleted: we

Deleted: y

Deleted: Moreover, c

Deleted: grid

Deleted: to

Deleted: biased

895 [factor of two, whereas the differences between observations and regional and global atmospheric chemistry models are frequently more than that \(Zhang et al., 2003; Hardacre et al., 2015; Clifton et al., 2017; Silva and Heald, 2017\). Furthermore,](#)  
900 [most of the site measurements in SynFlux are located in the US and Europe, mostly at midlatitudes. It is unclear how our results of dry deposition velocity and O<sub>3</sub> concentration would compare against observations in the tropics, which are relatively scarce compared to that at the midlatitudes.](#)

**Deleted:** (Ducker et al., 2018)

**Deleted:** ¶  
Another limitation is that we only validate our model against SynFlux. M

905 [Moreover, C<sub>4</sub> grass is ignored in our results because of a lack of site observations. The module also skipped the calculation for a PFT if it does not exist within the grid cell. This prohibited us from comparing model results to observations from the few C<sub>4</sub> grass sites. Extending the temporal length of simulations and including other sources of site observations may solve this problem. Utilizing the photosynthesis-based isoprene emission scheme to quantify feedback between atmospheric chemistry and vegetation via this specific pathway would also be a warranted follow-up of this development. Our current set of experiments only captured modest feedbacks between O<sub>3</sub> concentration and vegetation productivity via both the dry deposition and isoprene emission feedback pathways \(e.g., isoprene emission decreases following an O<sub>3</sub>-induced reduction in photosynthesis\), but did not consider how isoprene emission may respond immediately to acute O<sub>3</sub> exposure \(e.g., isoprene emission increases to counteract the oxidative stress from O<sub>3</sub>\) \(e.g., Loreto and Schnitzler, 2010\). As newer approaches to model O<sub>3</sub> damage on vegetation are available \(e.g., using a leaf mass-based index as suggested by Feng et al., 2018\), our model can](#)  
910 [provide a flexible framework for future studies to compare between the effects of different O<sub>3</sub> damage schemes on O<sub>3</sub>-vegetation interactions.](#) Comparing between different land cover inputs and evaluating the sensitivity of stomatal conductance and GPP to meteorological inputs under the new formulations using broader sources of data (e.g., satellite-derived GPP products) also warrant further investigation.

**Deleted:**

**Deleted:** Furthermore, u

#### **Author contribution**

JCYL wrote the source code of the ecophysiology module, conducted the model experiments and drafted the manuscript. APKT conceived the study, supervised the project, and cowrote the manuscript. JAD and CDH provided the datasets for model evaluation and supervised the writing of the manuscript.

925

#### **Code and/or Data Availability**

The code for the GEOS-Chem ecophysiology module and the data therein can be found in the Zenodo repository: <https://doi.org/10.5281/zenodo.7017973>

#### **930 Acknowledgements**

This work was supported by the Research Grants Council (RGC) General Research Fund (GRF; Proj. No.: 14306220) awarded to A. P. K. Tai.

## References

- 935 Ainsworth, E. A., Yendrek, C. R., Sitch, S., Collins, W. J. and Emberson, L. D.: The Effects of Tropospheric Ozone on Net Primary Productivity and Implications for Climate Change, *Annual Review of Plant Biology*, 63, 637–661, doi:10.1146/annurev-arplant-042110-103829, 2012.
- Anenberg, S. C., Horowitz, L. W., Tong, D. Q. and West, J. J.: An estimate of the global burden of anthropogenic ozone and fine particulate matter on premature human mortality using atmospheric modeling, *Environ. Health Perspect.*, 118, 1189–1195, doi:10.1289/ehp.0901220, 2010.
- 940 Arneth, A., Niinemets, Ü., Pressley, S., Bäck, J., Hari, P., Karl, T., Noe, S., Prentice, I. C., Serça, D., Hickler, T., Wolf, A. and Smith, B.: Process-based estimates of terrestrial ecosystem isoprene emissions: incorporating the effects of a direct CO<sub>2</sub>-isoprene interaction, *Atmos. Chem. Phys.*, 7, 31–53, doi:10.5194/acp-7-31-2007, 2007.
- Arneth, A., Monson, R. K., Schurgers, G., Niinemets, Ü., and Palmer, P. I.: Why are estimates of global terrestrial isoprene emissions so similar (and why is this not so for monoterpenes)?, *Atmos. Chem. Phys.*, 8, 4605–4620, <https://doi.org/10.5194/acp-8-4605-2008>, 2008.
- Avnery, S., Mauzerall, D. L., Liu, J. and Horowitz, L. W.: Global crop yield reductions due to surface ozone exposure: 1. Year 2000 crop production losses and economic damage, *Atmos. Environ.*, 45, 2284–2296, doi:https://doi.org/10.1016/j.atmosenv.2010.11.045, 2011.
- 950 Best, M., Pryor, M., Clark, D., Rooney, G., Essery, R., Ménard, C., Edwards, J., Hendry, M., Porson, A., Gedney, N., Mercado, L., Sitch, S., Blyth, E., Boucher, O., Cox, P., Grimmond, C. and Harding, R.: The Joint UK Land Environment Simulator (JULES), model description - Part 1: Energy and water fluxes, *Geosci. Model Dev.*, 4, 677, doi:10.5194/gmd-4-677-2011, 2011.
- Bey, I., Jacob, D., Yantosca, R., Logan, J., Field, B., Fiore, A., Li, Q., Liu, H., Mickley, L. and Schultz, M.: Global modeling of tropospheric chemistry with assimilated meteorology: Model description and evaluation, *J. Geophys. Res.-Atmos.*, 106, 23073–23095, doi:10.1029/2001JD000807, 2001.
- [Blyth, E., Clark, D. B., Ellis, R., Huntingford, C., Los, S., Pryor, M., Best, M., and Sitch, S.: A comprehensive set of benchmark tests for a land surface model of simultaneous fluxes of water and carbon at both the global and seasonal scale, \*Geosci. Model Dev.\*, 4, 255–269, doi:10.5194/gmd-4-255-2011, 2011.](#)
- 960 Bonan, G.: *Ecological Climatology: Concepts and Applications*, 3rd ed., Cambridge University Press, Cambridge, 2015.
- Clark, D., Mercado, L., Sitch, S., Jones, C., Gedney, N., Best, M., Pryor, M., Rooney, G., Essery, R., Blyth, E., Boucher, O., Harding, R., Huntingford, C. and Cox, P.: The Joint UK Land Environment Simulator (JULES), model description - Part 2: Carbon fluxes and vegetation dynamics, *Geosci. Model Dev.*, 4, 701, doi:10.5194/gmd-4-701-2011, 2011.
- [Clifton, O. E., Fiore, A. M., Munger, J. W., Malyshev, S., Horowitz, L. W., Shevliakova, E., Paulot, F., Murray, L. T., and Griffin, K. L.: Interannual variability in ozone removal by a temperate deciduous forest, \*Geophys. Res. Lett.\*, 44, 542–552, doi:10.1002/2016GL070923, 2017.](#)
- 965

- Collatz, G. J., Ball, J. T., Grivet, C. and Berry, J. A.: Physiological and environmental regulation of stomatal conductance, photosynthesis and transpiration: a model that includes a laminar boundary layer, *Agr. Forest Meteorol.*, 54, 107–136, doi:10.1016/0168-1923(91)90002-8, 1991.
- 970 Collatz, G., Ribas-Carbo, M. and Berry, J.: Coupled Photosynthesis-Stomatal Conductance Model for Leaves of C<sub>4</sub> Plants, *Aust. J. Plant Physiol.*, 19, 519–538, 1992.
- Cox, P. M., Huntingford, C. and Harding, R. J.: A canopy conductance and photosynthesis model for use in a GCM land surface scheme, *J. Hydrol.*, 212, 79–94, doi:10.1016/S0022-1694(98)00203-0, 1998.
- De Kauwe, M. G., Kala, J., Lin, Y.-S., Pitman, A. J., Medlyn, B. E., Duursma, R. A., Abramowitz, G., Wang, Y.-P. and  
 975 Miralles, D. G.: A test of an optimal stomatal conductance scheme within the CABLE land surface model, *Geosci. Model Dev.*, 8, 431, doi:10.5194/gmd-8-431-2015, 2015.
- [Dirmeyer, P. A., Gao, X., Zhao, M., Guo, Z., Oki, T., and Hanasaki, N.: GSWP-2: Multimodel analysis and implications for our perception of the land surface, \*B. Am. Meteorol. Soc.\*, 87, 1381–1397, doi:10.1175/BAMS-87-10-1381, 2006.](#)
- Ducker, J. A., Holmes, C. D., Keenan, T. F., Fares, S., Goldstein, A. H., Mammarella, I., Munger, J. W. and Schnell, J.:  
 980 Synthetic ozone deposition and stomatal uptake at flux tower sites, *Biogeosciences*, 15, 5395–5413, doi:10.5194/bg-15-5395-2018, 2018.
- Emberson, L. D., Kitwiroon, N., Beevers, S., Büker, P. and Cinderby, S.: Scorched Earth: how will changes in the strength of the vegetation sink to ozone deposition affect human health and ecosystems?, *Atmos. Chem. Phys.*, 13, 6741, doi:10.5194/acp-13-6741-2013, 2013.
- 985 [Feng, Z., Büker, P., Pleijel, H., Emberson, L., Karlsson, P. E., and Uddling, J.: A unifying explanation for variation in ozone sensitivity among woody plants, \*Glob. Chang. Biol.\*, 24\(1\), 78-84, doi:10.1111/gcb.13824, 2018.](#)
- Franks, P. J. and Farquhar, G. D.: A relationship between humidity response, growth form and photosynthetic operating point in C<sub>3</sub> plants, *Plant Cell Environ.*, 22, 1337–1349, doi:10.1046/j.1365-3040.1999.00494.x, 1999.
- Franks, P. J., Adams, M. A., Amthor, J. S., Barbour, M. M., Berry, J. A., Ellsworth, D. S., Farquhar, G. D., Ghannoum, O.,  
 990 Lloyd, J., McDowell, N., Norby, R. J., Tissue, D. T. and Caemmerer, S.: Sensitivity of plants to changing atmospheric CO<sub>2</sub> concentration: from the geological past to the next century, *New Phytol.*, 197, 1077–1094, doi:10.1111/nph.12104, 2013.
- Gelaro, R., McCarty, W., Suárez, M. J., Todling, R., Molod, A., Takacs, L., Randles, C. A., Darmenov, A., Bosilovich, M. G., Reichle, R., Wargan, K., Coy, L., Cullather, R., Draper, C., Akella, S., Buchard, V., Conaty, A., da Silva, A. M., Gu, W., Kim, G.-K., Koster, R., Lucchesi, R., Merkova, D., Nielsen, J. E., Partyka, G., Pawson, S., Putman, W., Rienecker, M., Schubert, S.  
 995 D., Sienkiewicz, M. and Zhao, B.: The Modern-Era Retrospective Analysis for Research and Applications, Version 2 (MERRA-2), *J. Climate*, 30, 5419–5454, doi:10.1175/JCLI-D-16-0758.1, 2017.
- Guenther, A. B., Jiang, X., Heald, C. L., Sakulyanontvittaya, T., Duhl, T., Emmons, L. K. and Wang, X.: The Model of Emissions of Gases and Aerosols from Nature version 2.1 (MEGAN2.1): an extended and updated framework for modeling biogenic emissions, *Geosci. Model Dev.*, 5(6), 1471–1492, doi:10.5194/gmd-5-1471-2012, 2012.

Deleted: .

- Hardacre, C., Wild, O., and Emberson, L.: An evaluation of ozone dry deposition in global scale chemistry climate models, *Atmos. Chem. Phys.*, 15, 6419–6436, doi:10.5194/acp-15-6419-2015, 2015.
- Harper, A. B., Williams, K. E., McGuire, P. C., Duran Rojas, M. C., Hemming, D., Verhoef, A., Huntingford, C., Rowland, L., Marthews, T., Breder Eller, C., Mathison, C., Nobrega, R. L. B., Gedney, N., Vidale, P. L., Otu-Larbi, F., Pandey, D., Garrigues, S., Wright, A., Slevin, D., De Kauwe, M. G., Blyth, E., Ardö, J., Black, A., Bonal, D., Buchmann, N., Burban, B., Fuchs, K., de Grandcourt, A., Mammarella, I., Merbold, L., Montagnani, L., Nouvellon, Y., Restrepo-Coupe, N., and Wohlfahrt, G.: Improvement of modeling plant responses to low soil moisture in JULESv4.9 and evaluation against flux tower measurements, *Geosci. Model Dev.*, 14, 3269–3294, doi:10.5194/gmd-14-3269-2021, 2021.
- Hoesly, R. M., Smith, S. J., Feng, L., Klimont, Z., Janssens-Maenhout, G., Pitkanen, T., Seibert, J. J., Vu, L., Andres, R. J., Bolt, R. M., Bond, T. C., Dawidowski, L., Kholod, N., Kurokawa, J.-I., Li, M., Liu, L., Lu, Z., Moura, M. C. P., O'Rourke, P. R. and Zhang, Q.: Historical (1750–2014) anthropogenic emissions of reactive gases and aerosols from the Community Emissions Data System (CEDS), *Geosci. Model Dev.*, 11, 369–408, doi:10.5194/gmd-11-369-2018, 2018.
- Huang, L., McDonald-Buller, E. C., McGaughey, G., Kimura, Y. and Allen, D. T.: The impact of drought on ozone dry deposition over eastern Texas, *Atmos. Environ.*, 127, 176–186, doi:https://doi.org/10.1016/j.atmosenv.2015.12.022, 2016.
- Huntingford, C., Oliver, R. J., Mercado, L. M., and Sitch, S.: Technical note: A simple theoretical model framework to describe plant stomatal “sluggishness” in response to elevated ozone concentrations, *Biogeosciences*, 15, 5415–5422, https://doi.org/10.5194/bg-15-5415-2018, 2018.
- Jacob, D. J. and Winner, D. A.: Effect of climate change on air quality, *Atmos. Environ.*, 43, 51-63, doi:10.1016/j.atmosenv.2008.09.051, 2009.
- Jarvis, P. G.: Interpretation of Variations in Leaf Water Potential and Stomatal Conductance Found in Canopies in Field, *Philosophical Transactions of the Royal Society of London Series B-Biological Sciences*, 273, 593-610, doi:DOI 10.1098/rstb.1976.0035, 1976.
- Kavassalis, S. C. and Murphy, J. G.: Understanding ozone-meteorology correlations: A role for dry deposition, *Geophys. Res. Lett.*, 44, 2922–2931, doi:10.1002/2016GL071791, 2017.
- Keller, C. A., Long, M. S., Yantosca, R. M., Da Silva, A. M., Pawson, S., and Jacob, D. J.: HEMCO v1.0: a versatile, ESMF-compliant component for calculating emissions in atmospheric models, *Geosci. Model Dev.*, 7, 1409–1417, https://doi.org/10.5194/gmd-7-1409-2014, 2014.
- Koster, R. D., Guo, Z., Yang, R., Dirmeyer, P. A., Mitchell, K., and Puma, M. J.: On the Nature of Soil Moisture in Land Surface Models, *J. Climate*, 22, 4322–4335, doi:10.1175/2009JCLI2832.1, 2009.
- Lei, Y., Yue, X., Liao, H., Gong, C. and Zhang, L.: Implementation of Yale Interactive terrestrial Biosphere model v1.0 into GEOS-Chem v12.0.0: a tool for biosphere–chemistry interactions, *Geosci. Model Dev.*, 13, 1137–1153, doi:10.5194/gmd-13-1137-2020, 2020.

- Leuning, R.: A critical appraisal of a combined stomatal-photosynthesis model for C<sub>3</sub> plants, *Plant Cell Environ.*, 18, 339–355, doi:10.1111/j.1365-3040.1995.tb00370.x, 1995.
- 1035 Lombardozi, D., Levis, S., Bonan, G., Hess, P. G. and Sparks, J. P.: The Influence of Chronic Ozone Exposure on Global Carbon and Water Cycles, *J. Climate*, 28, 292–305, doi:10.1175/JCLI-D-14-00223.1, 2015.
- Loreto, F. and Schnitzler, J.-P., Abiotic stresses and induced BVOCs, *Trends in Plant Sci.*, 15, 154-156, doi: 10.1016/j.tplants.2009.12.006, 2010.
- Medlyn, B. E., Duursma, R. A., Eamus, D., Ellsworth, D. S., Prentice, I. C., Barton, C. V. M., Crous, K. Y., De Angelis, P., 1040 Freeman, M. and Wingate, L.: Reconciling the optimal and empirical approaches to modelling stomatal conductance, *Global Change Biol.*, 17, 2134–2144, doi:10.1111/j.1365-2486.2010.02375.x, 2011.
- [Mills G., Pleijel H., Malley C. S., Sinha B., Cooper O. R., Schultz M. G., Neufeld H. S., Simpson D., Sharps K., Feng Z., Gerosa G., Harmens H., Kobayashi K., Saxena P., Paoletti E., Sinha V., Xu X.: Tropospheric Ozone Assessment Report: Present-day tropospheric ozone distribution and trends relevant to vegetation, \*Elementa: Science of the Anthropocene\*, 6, 47, doi:10.1525/elementa.302, 2018.](#)
- 1045 Monson, R. and Baldocchi, D.: *Terrestrial Biosphere-Atmosphere Fluxes*, Cambridge University Press, Cambridge., 2014.
- Pacifico, F., Harrison, S. P., Jones, C. D., Arnth, A., Sitch, S., Weedon, G. P., Barkley, M. P., Palmer, P. I., Serça, D., Potosnak, M., Fu, T.-M., Goldstein, A., Bai, J., and Schurgers, G.: Evaluation of a photosynthesis-based biogenic isoprene emission scheme in JULES and simulation of isoprene emissions under present-day climate conditions, *Atmos. Chem. Phys.*, 11, 4371–4389, doi:10.5194/acp-11-4371-2011, 2011.
- 1050 Possell, M. and Hewitt, C. N.: Isoprene emissions from plants are mediated by atmospheric CO<sub>2</sub> concentrations, *Global Change Biol.*, 17, 1595–1610, doi:10.1111/j.1365-2486.2010.02306.x, 2011.
- [Pound, R. J., Sherwen, T., Helmig, D., Carpenter, L. J., and Evans, M. J.: Influences of oceanic ozone deposition on tropospheric photochemistry, \*Atmos. Chem. Phys.\*, 20, 4227–4239, doi:10.5194/acp-20-4227-2020, 2020.](#)
- 1055 [Powell, T. L., Galbraith, D. R., Christoffersen, B. O., Harper, A., Imbuzeiro, H. M. A., Rowland, L., Almeida, S., Brando, P. M., da Costa, A. C. L., Costa, M. H., Levine, N. M., Malhi, Y., Saleska, S. R., Sotta, E., Williams, M., Meir, P., and Moorcroft, P. R.: Confronting model predictions of carbon fluxes with measurements of Amazon forests subjected to experimental drought, \*New Phytol.\*, 200, 350–365, doi:10.1111/nph.12390, 2013.](#)
- Prather, M. J. and Ehhalt, D.: *Atmospheric Chemistry and Greenhouse Gases*, edited by J. T. Houghton, Y. Ding, and D. J. Griggs, Cambridge University Press, Cambridge., 2001.
- 1060 Raoult, N. M., Jupp, T. E., Cox, P. M. and Luke, C. M.: Land-surface parameter optimisation using data assimilation techniques: the adJULES system V1.0, *Geosci. Model Dev.*, 9, 2833, doi:10.5194/gmd-9-2833-2016, 2016.
- Ronan, A. C., Ducker, J. A., Schnell, J. L., and Holmes, C. D.: Have improvements in ozone air quality reduced ozone uptake into plants? *Elem Sci Anth*, 8, 2, doi:10.1525/elementa.399, 2020.



- 1065 Sadiq, M., Tai, A. P. K., Lombardozi, D. and Val Martin, M.: Effects of ozone–vegetation coupling on surface ozone air quality via biogeochemical and meteorological feedbacks, *Atmos. Chem. Phys.*, 17, 3055–3066, doi:10.5194/acp-17-3055-2017, 2017.
- Sanderson, M. G., Jones, C. D., Collins, W. K., Johnson, C. E. and Derwent, R. G.: Effect of Climate Change on Isoprene Emissions and Surface Ozone Levels, *Geophys. Res. Lett.*, 30, 1936, doi:10.1029/2003GL017642, 2003.
- 1070 Sanderson, M. G., Collins, W. J., Hemming, D. L. and Betts, R. A.: Stomatal conductance changes due to increasing carbon dioxide levels: Projected impact on surface ozone levels, *Tellus B: Chemical and Physical Meteorology*, 59, 404–411, doi:10.1111/j.1600-0889.2007.00277.x, 2007.
- Sellers, P. J., Randall, D. A., Collatz, G. J., Berry, J. A., Field, C. B., Dazlich, D. A., Zhang, C., Collelo, G. D. and Bounoua, L.: A Revised Land Surface Parameterization (SiB2) for Atmospheric GCMs. Part I: Model Formulation, *J. Climate*, 9, 676–1075 705, 1996.
- Sitch, S., Cox, P. M., Collins, W. J. and Huntingford, C.: Indirect radiative forcing of climate change through ozone effects on the land-carbon sink, *Nature*, 448, 791, doi:10.1038/nature06059, 2007.
- [Silva, S. J. and Heald, C. L.: Investigating dry deposition of ozone to vegetation, \*J. Geophys. Res.-Atmos.\*, 123, 559–573, https://doi.org/10.1002/2017JD027278, 2018.](https://doi.org/10.1002/2017JD027278)
- 1080 Slevin, D., Tett, S. F. B., Exbrayat, J.-F., Bloom, A. A. and Williams, M.: Global evaluation of gross primary productivity in the JULES land surface model v3.4.1, *Geosci. Model Dev.*, 10, 2651, doi:10.5194/gmd-10-2651-2017, 2017.
- Stevenson, D. S., Dentener, F. J., Schultz, M. G., Ellingsen, K., van Noije, T. P. C., Wild, O., Zeng, G., Amann, M., Atherton, C. S., Bell, N., Bergmann, D. J., Bey, I., Butler, T., Cofala, J., Collins, W. J., Derwent, R. G., Doherty, R. M., Drevet, J., Eskes, H. J., Fiore, A. M., Gauss, M., Hauglustaine, D. A., Horowitz, L. W., Isaksen, I. S. A., Krol, M. C., Lamarque, J.-F., Lawrence, 1085 M. G., Montanaro, V., Müller, J.-F., Pitari, G., Prather, M. J., Pyle, J. A., Rast, S., Rodriguez, J. M., Sanderson, M. G., Savage, N. H., Shindell, D. T., Strahan, S. E., Sudo, K. and Szopa, S.: Multimodel ensemble simulations of present-day and near-future tropospheric ozone, *J. Geophys. Res.*, 111, doi:10.1029/2005JD006338, 2006.
- Tai, A. P. K., Mickley, L. J., Heald, C. L. and Wu, S.: Effect of CO<sub>2</sub> inhibition on biogenic isoprene emission: Implications for air quality under 2000 to 2050 changes in climate, vegetation, and land use, *Geophys. Res. Lett.*, 40, 3479–3483, 1090 doi:10.1002/grl.50650, 2013.
- Tai, A. P. K., Martin, M. V. and Heald, C. L.: Threat to future global food security from climate change and ozone air pollution, *Nature Climate Change*, 4, 817–821, doi:10.1038/nclimate2317, 2014.
- Tai, A. P. K. and Val Martin, M.: Impacts of ozone air pollution and temperature extremes on crop yields: Spatial variability, adaptation and implications for future food security, *Atmos. Environ.*, 169, 11–21, doi:https://doi.org/10.1016/j.atmosenv.2017.09.002, 2017.
- 1095

- Travis, K. R., Jacob, D. J., Fisher, J. A., Kim, P. S., Marais, E. A., Zhu, L., Yu, K., Miller, C. C., Yantosca, R. M., Sulprizio, M. P., and Thompson, A.M. Why do models overestimate surface ozone in the southeastern United States? *Atmos. Chem. Phys.*, 16(21), 13561-13577, doi:10.5194/acp-16-13561-2016, 2016.
- Trugman, A. T., Medvigy, D., Mankin, J. S. and Anderegg, W. R. L.: Soil Moisture Stress as a Major Driver of Carbon Cycle Uncertainty, *Geophys. Res. Lett.*, 45, 6495–6503, doi:10.1029/2018GL078131, 2018.
- Unger, N.: Isoprene emission variability through the twentieth century, *J. Geophys. Res.-Atmos.*, 118, 13,606-13,613, doi:10.1002/2013JD020978, 2013.
- [Verhoef, A. and Egea, G.: Modeling plant transpiration under limited soil water: Comparison of different plant and soil hydraulic parameterizations and preliminary implications for their use in land surface models. \*Agr. Forest Meteorol.\*, 191, 22–32, doi:10.1016/j.agrformet.2014.02.009, 2014.](#)
- Wang, L., Tai, A. P. K., Tam, C. Y., Sadiq, M., Wang, P., and Cheung, K. K. W.: Impacts of future land use and land cover change on mid-21st-century surface ozone air quality: distinguishing between the biogeophysical and biogeochemical effects, *Atmos. Chem. Phys.*, 20, 11349-11369, doi:10.5194/acp-20-11349-2020, 2020.
- Weng, H., Lin, J., Martin, R., Millet, D., Jaeglé, L., Ridley, D., Keller, C., Li, C., Du, M., Meng, J.: Global high-resolution emissions of soil NO<sub>x</sub>, sea salt aerosols, and biogenic volatile organic compounds, *Sci Data* 7, 148, doi.org:10.1038/s41597-020-0488-5, 2020.
- Wesely, M. L.: Parameterization of surface resistances to gaseous dry deposition in regional-scale numerical models, *Atmos. Environ.*, 23, 1293–1304, doi:10.1016/0004-6981(89)90153-4, 1989.
- Wild, O.: Modelling the global tropospheric ozone budget: exploring the variability in current models, *Atmos. Chem. Phys.*, 7, 2643–2660, doi:10.5194/acp-7-2643-2007, 2007.
- Wong, A. Y. H., Geddes, J. A., Tai, A. P. K. and Silva, S. J.: Importance of dry deposition parameterization choice in global simulations of surface ozone, *Atmos. Chem. Phys.*, 19, 14365–14385, doi:10.5194/acp-19-14365-2019, 2019.
- [Yuan, H., Dai, Y., Xiao, Z., Ji, D. and Shangguan, W.: Reprocessing the MODIS Leaf Area Index products for land surface and climate modelling, \*Remote Sens. Environ.\*, 115, 1171–1187, doi:https://doi.org/10.1016/j.rse.2011.01.001, 2011.](#)
- Yue, X. and Unger, N.: The Yale Interactive terrestrial Biosphere model version 1.0: description, evaluation and implementation into NASA GISS ModelE2, *Geosci. Model Dev.*, 8, 2399–2417, doi:10.5194/gmd-8-2399-2015, 2015.
- Zhang, L., Brook, J. R. and Vet, R.: A revised parameterization for gaseous dry deposition in air-quality models, *Atmos. Chem. Phys.*, 3, 2067–2082, doi:10.5194/acp-3-2067-2003, 2003.
- Zhou, S. S., Tai, A. P. K., Sun, S., Sadiq, M., Heald, C. L. and Geddes, J. A.: Coupling between surface ozone and leaf area index in a chemical transport model: strength of feedback and implications for ozone air quality and vegetation health, *Atmos. Chem. Phys.*, 18, 14133–14148, doi:10.5194/acp-18-14133-2018, 2018.

**Deleted:** Young, P.J., Naik, V., Fiore, A.M., Gaudel, A., Guo, J., Lin, M.Y., Neu, J.L., Parrish, D.D., Rieder, H.E., Schnell, J.L., Tilmes, S., Wild, O., Zhang, L., Ziemke, J.R., Brandt, J., Delcloo, A., Doherty, R.M., Geels, C., Hegglin, M.I., Hu, L., Im, U., Kumar, R., Luhar, A., Murray, L., Plummer, D., Rodriguez, J., Saiz-Lopez, A., Schultz, M.G., Woodhouse, M.T. and Zeng, G.: Tropospheric Ozone Assessment Report: Assessment of global-scale model performance for global and regional ozone distributions, variability, and trends. *Elem Sci Anth*, 6(1), 10, doi:10.1525/elementa.265, 2018.\*

